

Alfvén: magnetosphere—ionosphere connection explorers

M. Berthomier · A. N. Fazakerley · C. Forsyth · R. Pottelette · O. Alexandrova · A. Anastasiadis · A. Aruliah · P.-L. Blelly · C. Briand · R. Bruno · P. Canu · B. Cecconi · T. Chust · I. Daglis · J. Davies · M. Dunlop · D. Fontaine · V. Génot · B. Gustavsson · G. Haerendel · M. Hamrin · M. Hapgood · S. Hess · D. Kataria · K. Kauristie · S. Kemble · Y. Khotyaintsev · H. Koskinen · L. Lamy · B. Lanchester · P. Louarn · E. Lucek · R. Lundin · M. Maksimovic · J. Manninen · A. Marchaudon · O. Marghitsu · G. Marklund · S. Milan · J. Moen · F. Mottez · H. Nilsson · N. Ostgaard · C. J. Owen · M. Parrot · A. Pedersen · C. Perry · J.-L. Pinçon · F. Pitout · T. Pulkkinen · I. J. Rae · L. Rezeau · A. Roux · I. Sandahl · I. Sandberg · E. Turunen · J. Vogt · A. Walsh · C. E. J. Watt · J. A. Wild · M. Yamauchi · P. Zarka · I. Zouganelis

Received: 31 March 2011 / Accepted: 6 November 2011 / Published online: 27 December 2011
© Springer Science+Business Media B.V. 2011

Abstract The aurorae are dynamic, luminous displays that grace the night skies of Earth's high latitude regions. The solar wind emanating from the Sun is their ultimate energy source, but the chain of plasma physical processes leading to auroral displays is complex. The special conditions at the interface between

Prof Ingrid Sandahl passed away on May 5, 2011.

M. Berthomier · R. Pottelette · I. Zouganelis
Laboratoire de Physique des Plasmas (LPP), Observatoire de St Maur, 4 avenue de Neptune,
94107 Saint-Maur des Fossés Cedex, France

A. N. Fazakerley (✉) · C. Forsyth · D. Kataria · C. J. Owen · A. Walsh
Mullard Space Science Laboratory, University College London,
Holmbury St. Mary, Dorking, Surrey, RH5 6NT, UK
e-mail: anf@mssl.ucl.ac.uk

O. Alexandrova · C. Briand · B. Cecconi · S. Hess · L. Lamy · M. Maksimovic · P. Zarka
Laboratoire d'Études Spatiales et d'Instrumentation Astrophysique (LESIA),
Observatoire de Paris, 5 place Jules Janssen, 92190 Meudon Cedex, France

P. Canu · T. Chust · D. Fontaine · L. Rezeau · A. Roux
Laboratoire de Physique des Plasmas (LPP/CNRS), Ecole Polytechnique, Route de Saclay,
91128 Palaiseau Cedex, France

A. Anastasiadis · I. Daglis · I. Sandberg
Institute for Space Applications and Remote Sensing (ISARS),
National Observatory of Athens, Vas. Pavlou & I. Metaxa, Penteli, Athens 15236, Greece

the solar wind-driven magnetosphere and the ionospheric environment at the top of Earth's atmosphere play a central role. In this Auroral Acceleration Region (AAR) persistent electric fields directed along the magnetic field accelerate magnetospheric electrons to the high energies needed to excite luminosity when they hit the atmosphere. The “ideal magnetohydrodynamics” description of space plasmas which is useful in much of the magnetosphere cannot be used to understand the AAR. The AAR has been studied by a small number of single spacecraft missions which revealed an environment rich in wave-particle interactions, plasma turbulence, and nonlinear acceleration processes, acting on a variety of spatio-temporal scales. The pioneering 4-spacecraft Cluster magnetospheric research mission is now fortuitously visiting the AAR, but its particle instruments are too slow to allow resolve many of the key plasma physics phenomena. The Alfvén concept is designed specifically to take the next step in studying the aurora, by making the crucial high-time resolution, multi-scale measurements in the AAR, needed to address the

A. Aruliah

Atmospheric Physics Laboratory (APL), Department of Physics and Astronomy,
University College London, Gower Street, London, UK

P.-L. Blelly · V. Génot · P. Louarn · F. Pitout

Institut de Recherche en Astrophysique et Planétologie (IRAP),
9, avenue du Colonel Roche, BP 44346, 31028 Toulouse Cedex 4, France

R. Bruno

Institute of Physics of Interplanetary Space, INAF, Via del Fosso del Cavaliere,
10000133 Rome, Italy

J. Davies · M. Dunlop · M. Hapgood · C. Perry

Rutherford Appleton Laboratory (RAL), STFC, Harwell, Didcot, UK

B. Gustavsson · B. Lanchester

Space Environment Physics Group, School of Physics and Astronomy,
University of Southampton, Southampton, Hampshire, UK

G. Haerendel

Max-Planck-Institut für extraterrestrische Physik, Giessenbachstrasse,
85748 Garching, Germany

M. Hamrin

Department of Physics, Umea University, 901 87 Umea, Sweden

K. Kauristie · H. Koskinen

Space Research Unit, Finnish Meteorological Institute (FMI), PO Box 503,
00101, Helsinki, Finland

S. Kemble

EADS Astrium, Stevenage, Hertfordshire, UK

key science questions of auroral plasma physics. The new knowledge that the mission will produce will find application in studies of the Sun, the processes that accelerate the solar wind and that produce aurora on other planets.

Keywords Alfvén · Cosmic vision · Auroral acceleration region · Space plasmas

1 Introduction

The Alfvén mission concept proposes a new strategy for investigating universal plasma physical processes that govern what Nobel laureate Hannes Alfvén named “The Plasma Universe”. Such processes encompass the *acceleration of charged particles* connected to the *generation of electromagnetic radiation*, the development of *strong plasma turbulence* associated with the *maintenance of parallel electric fields* along magnetic field lines in a collisionless plasma, and complex ion heating phenomena leading to *planetary ion outflow*. The most

Y. Khotyaintsev

Angstrom Laboratory, Swedish Institute of Space Physics (IRF), Box 537,
751 21 Uppsala, Sweden

E. Lucek

Space and Atmospheric Physics Group, The Blackett Laboratory, Imperial College London,
Prince Consort Road, London, UK

R. Lundin · H. Nilsson · I. Sandahl · M. Yamauchi

Swedish Institute of Space Physics (IRF), Box 812, 981 92 Kiruna, Sweden

J. Manninen

Sodankyla Geophysical Observatory (SGO), University of Oulu, Tähteläntie 62,
99600 Sodankyla, Finland

A. Marchaudon · M. Parrot · J.-L. Pinçon

Laboratoire de Physique et Chimie de l'Environnement et de l'Espace (LPC2E), CNRS,
3A, Avenue de la Recherche Scientifique, 45071 Orléans Cedex 2, France

O. Marghita

Institute for Space Sciences (ISS), P.O.Box MG-23, 077125, Bucharest-Magurele, Romania

G. Marklund

Division of Plasma Physics, Alfvén Laboratory, KTH, Royal Institute of Technology,
Teknikringen 31, 100 44 Stockholm, Sweden

S. Milan

Radio and Space Plasma Physics, Department of Physics and Astronomy,
University of Leicester, University Road, Leicester, UK

J. Moen · A. Pedersen

Plasma and Space Physics Group, Department of Physics, University of Oslo,
Postboks 1048, Blindern 0316 Oslo, Norway

accessible regions of space for the study of these processes are the auroral regions of the Earth's magnetosphere.

The auroral regions are a key region of our solar system: they constitute the interface that connects the distant solar wind-driven collisionless magnetosphere to the much denser ionospheric environment at the top of Earth's atmosphere. A significant fraction of the energy fed in by the solar wind to the magnetosphere is dissipated in this interface, often explosively during magnetic substorms. In this transition region, the plasma organizes itself on small spatial and fast temporal scales. The Auroral Acceleration Region (AAR) has been previously studied by a small number of single spacecraft: S3-3 (1976), DE-1 (1981), Viking (1986), Freja (1992), Polar (1995) and FAST (1996). High-time resolution FAST instruments revealed a plasma physics environment rich in wave-particle interactions, plasma turbulence, and nonlinear acceleration processes, which implied a variety of spatio-temporal scales. ESA's pioneering multi-spacecraft Cluster mission is now exploring the AAR, revealing dramatic variability of large-scale auroral phenomena. Cluster can't be used to relate these to phenomena observed by FAST as its particle instruments are too slow.

Key science questions related to the efficiency of acceleration processes and to their ability to generate the complex features of auroral displays remain unanswered. In particular, high-time resolution observations have suggested that acceleration by Alfvén waves would be responsible for the generation of the sub-km scale auroral arcs. Single spacecraft measurements cannot evaluate the energy exchanged over a large volume of space between waves and particles. They cannot assess the efficiency of this mechanism, nor can they

F. Mottez

Laboratoire Univers et Théories (LUTH), Observatoire de Paris, 5 place Jules Janssen,
92195 Meudon cedex, France

N. Ostgaard

Departments of Physics and Technology, University of Bergen, Allegt 55,
5007 Bergen, Norway

T. Pulkkinen

School of Electrical Engineering, Aalto University, P.O. Box 13000, 00076 Aalto, Finland

I. J. Rae · C. E. J. Watt

Department of Physics, University of Alberta, Edmonton, AB, Canada

E. Turunen

EISCAT Headquarters, PO Box 812, SE-981 92 Kiruna, Sweden

J. Vogt

School of Engineering and Science, Jacobs University Bremen, P.O. Box 750561,
28725 Bremen, Germany

J. A. Wild

Space Plasma Environment and Radio Science Group, Department of Physics,
InfoLab21, Lancaster University, Lancaster, UK

tell us where and when it is effective and how it relates to the evolution of the magnetosphere—ionosphere connection. From high-time resolution particle data, it has been proposed that localized parallel electric fields would explain the larger scale arcs that can be observed by onboard imagers and that are associated with large scale current structures that connect the magnetosphere to the ionosphere. Single spacecraft measurements cannot follow the formation and evolution of these transient structures or the complex transport phenomena associated with the strong plasma turbulence that develop along magnetic field lines around these structures. Fundamental questions about auroral kilometric radiation, its propagation and its fine structure, and about highly variable and diverse ionospheric ion outflows, remain unanswered by earlier missions.

The Alfvén mission will be the first mission to combine high-time resolution and multi-scale measurements in the AAR. It will fly through the heart of the AAR between a few 1,000 and 8,000 km altitude with two manoeuvrable spacecraft. Each spacecraft will carry the same high-time resolution instrumentation. This is essential to allow appropriate inter-spacecraft correlations and to solve the key science questions of auroral plasma physics. Thanks to the high-resolution auroral imager present on both spacecraft, this mission will offer a truly outstanding opportunity to unveil the mysteries of auroral displays. These unique capabilities together with a strong coordination with the existing network of ground based observatories provide the opportunity to improve our understanding of the magnetosphere—ionosphere connection. At the same time, the Alfvén mission will allow Europe to achieve a real breakthrough in the physics of hot collisionless plasmas. The near-Earth space plasma constitutes the most readily accessible cosmic plasma system available for extensive and detailed in situ observations of these physical phenomena. Dedicating this mission to Hannes Alfvén, we anticipate that it will not only tell us how our Solar System works but it will also provide a unified Cosmic Vision of our Plasma Universe.

2 Scientific objectives and requirements

2.1 Particle acceleration by Alfvén waves and the generation of small-scale auroral arcs

Auroral particle acceleration is a key topic in magnetospheric physics. Today there is a general consensus that both quasi-static and wave electric fields contribute to field-aligned electron acceleration in the collisionless auroral plasma. However, we have yet to establish whether these acceleration mechanisms can provide sufficient energy and flux to stimulate discrete arcs over a wide range of spatio-temporal scales, and the association between each acceleration process and specific patterns of magnetosphere-ionosphere coupling is unclear.

Shear Alfvén waves are low-frequency waves that can support such accelerating parallel electric fields when their perpendicular scale lengths are small enough. Single-point observations have associated short-scale shear Alfvén waves—also called Dispersive Alfvén Waves (DAW)—with accelerated electrons [1]. However, there are few studies which demonstrate that electrons might gain energy at the expense of the waves during a single event due to the non-local nature of the process that develops over large distances along the magnetic field. Measurements of particle and wave energy at more than one location along the magnetic field are needed to fully characterize the acceleration by Alfvén waves in the auroral regions. For example, Dombeck et al. [2] had to rely upon a fortuitous conjunction between the Polar and FAST satellites, in order to correctly diagnose that the acceleration mechanism was related to DAW. Given typical number density profiles, acceleration can occur over distances of hundreds or even thousands of kilometers along the magnetic field. Consequently, systematic observations of particle and wave energy by two magnetically conjugate spacecraft are needed to fully characterize the acceleration by Alfvén waves in the auroral regions.

2.1.1 How efficient is Alfvénic acceleration in producing small-scale arcs?

Numerical simulations indicate that Alfvénic electron acceleration can happen below 4,000 km where inertial effects dominate [e.g. 3], and at higher altitudes where electron pressure effects dominate [e.g. 4]. Depending on where and over which range of altitudes the Alfvénic acceleration takes place, this process will produce different electron energies and fluxes and auroral arcs of different widths and brightness [5]. Since the location of the acceleration is where the waves develop sufficiently short perpendicular scales, interferometry [e.g. 6] can be used to identify the perpendicular scales of the waves from electric and magnetic field measurements. This will show whether short perpendicular scales develop as the wave propagates along the field, or whether they have already developed at higher altitudes.

The Alfvén mission will supply this information by providing magnetic field conjunctions between two spacecraft in a large range of altitudes, from ~1,000 km to 8,000 km and at different latitudes and magnetic local times. The typical inter-spacecraft separation distance along the magnetic field should be of the order of 100 km to several 100's km. Observations of plasma characteristics including high-time resolution 2D electron pitch-angle measurements on a few 10's ms time scale at multiple locations will be needed to identify short bursts of accelerated electrons. The ability to distinguish between DAW and small-scale magnetic field-aligned currents is also very important in the topside ionosphere [7]. Electromagnetic field data are necessary to diagnose the properties of DAW, to perform Poynting flux measurements, and to assess the efficiency of the Alfvénic acceleration process. By combining these data with ground-based optical data from facilities in Scandinavia and in North America, we will be able to finally understand whether Alfvén waves can

feed sufficient energy into the electrons to create the small-scale (sub-km) arcs.

2.1.2 How do Alfvén waves dissipate in auroral density inhomogeneities?

Large scale density cavities (from ~ 10 km to a few 100's km across the magnetic field) are observed above the auroral oval. It has been suggested that Alfvén wave fronts propagating onto the edge of these cavities might distort which would lead to the formation of small perpendicular scales [8]. Numerical simulations have shown that the energy budget of the process delivers net electron acceleration and dissipation of the wave energy [9]. It is estimated that an Alfvén wave could be dissipated in a few seconds. Some aspects of this scenario have been tested using FAST observations in the topside ionosphere [10]. However, single spacecraft data cannot be used to analyse the full energy budget of this process. Also, the efficiency of this mechanism is highly dependent on the cavity configuration about which little is known from single spacecraft crossings.

The Alfvén mission will establish the role of auroral density inhomogeneities in generating accelerated electrons. During the parallel phase of the mission, it will be possible to quantify the Alfvén wave energy that is dissipated in density inhomogeneities. Typical inter-spacecraft distances ranging from ~ 100 km to several 100's km will be needed. During the transverse phase of the mission, when the two spacecraft will cross the edges of auroral cavities at different times, we will develop a better knowledge of the temporal evolution of the density gradients. The efficiency of the process heavily depends on the cavity lifetime which will be established by systematic crossings at different altitudes, from $\sim 1,000$ km up to at least one Earth radius, and with different delays between the spacecraft, from a few to several tens of seconds.

It will also be possible to identify cavity reformation processes: small scale secondary cavities may be excavated during DAW propagation and they might lead to subsequent dissipation and electron acceleration. Can the auroral system evolve from Alfvénic acceleration processes seen at the onset of a substorm (see next paragraph) to a quasi-static situation with particle acceleration through electrostatic structures such as strong double layers? If small-scale secondary cavities generated by dissipating DAW are a precursor of larger scale auroral cavities, then the Alfvén spacecraft will be able to observe this transition during the transverse phase of the mission.

2.1.3 Do Alfvén waves accelerate electrons during substorm expansion phase onset?

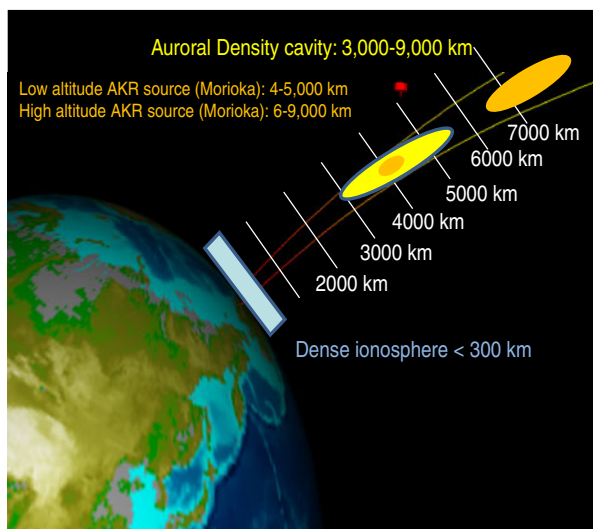
It is well known that stored energy transferred from the solar wind into near-Earth space is explosively released during substorm expansion phase onset, powering aurora and generating energetic particle populations [11]. The physics and the location of the region initiating the onset of the substorm expansion have remained controversial for decades [e.g., 12]. It is also well

known that in the ionosphere, the first indication of a substorm onset is a sudden brightening of one of the quiet arcs lying near the midnight sector of the oval (or a sudden formation of an arc). However, the source of accelerated electrons that are responsible for this auroral brightening is not clear, ~50 years following its discovery.

It has been suggested that broadband accelerated electron signatures are associated with Alfvén wave activity following substorm onset [e.g. 13]. Furthermore, Newell et al. [14] presented strong evidence that the electron energy flux from these broadband spectra increases significantly at substorm expansion phase onset. Rae et al. [15] demonstrate that ground-based observations of ULF wave amplitudes increase at the same time and in the same location as the first optical signatures of substorm expansion phase onset in the ionosphere. Interestingly, the onset and increase of ULF wave activity in the magnetosphere also occurs in close coincidence with the onset of ground magnetic activity [e.g., 16], providing a tantalising glimpse of the link between these ground-based perturbations and their possible magnetospheric counterparts. Taken together, these results suggest that ULF wave-activity, broadband aurora and substorm expansion phase onset may be intimately linked on short time scales, perhaps by the acceleration of electrons via shear Alfvén waves [e.g. 4].

The sudden formation of a parallel electric field is essential to complete substorm onset. This acceleration exhibits a two-step evolution as shown by auroral kilometric radiation observations [17]: the activation of low altitude acceleration (4–5,000 km) which corresponds to the initial auroral brightening, and subsequent abrupt breakout of high altitude acceleration (above 6,000 km) which corresponds to auroral breakup (see Fig. 1). During the parallel phase of the mission, measurements along the same field lines at two different altitudes

Fig. 1 Two-step evolution of the acceleration at substorm onset

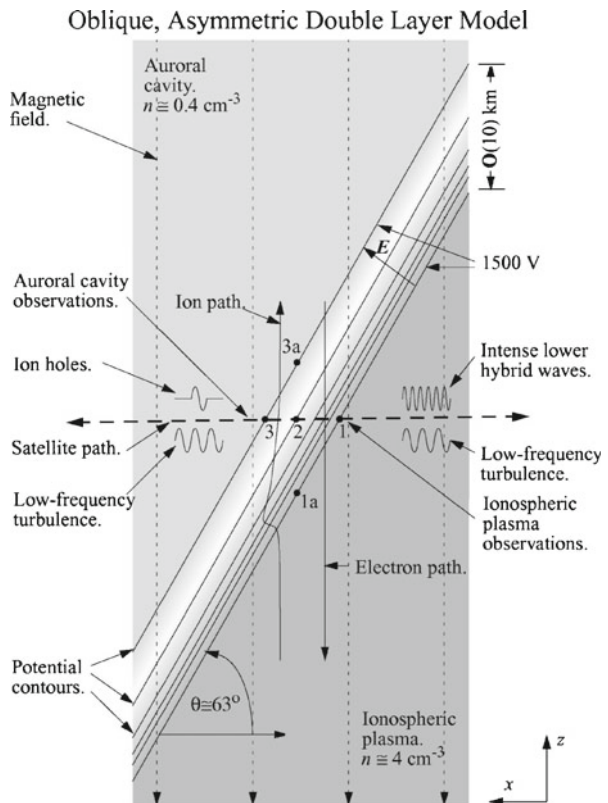


will show how electrons gain the energy required to power the aurora at substorm onset times. The in situ measurements must be made in regions of space conjugate to ground-based measurements of magnetic field and auroral imaging in order to put the measurements in the context of the global substorm evolution.

2.2 Parallel acceleration in magnetic field-aligned current structures

Among the complex current systems which connect the magnetosphere to the ionosphere, the auroral zone includes a region of quasi-stationary magnetic field-aligned currents where ion beams drift away from the ionosphere along magnetic field lines while energetic electrons travelling earthward “shower” the upper atmosphere. The associated inverted-V arcs are typically large scale and stable structures compared to those described in Section 2.1. At 3,000–4,000 km altitude, FAST satellite data have shown that a strong Double Layer (DL) localized within ten Debye lengths $\sim 1\text{--}10$ km marks the transition from the topside ionosphere to a so-called auroral cavity where the plasma is an order of magnitude more tenuous (see Fig. 2). Strong DLs associated with an electric field of opposite polarity have also been shown to exist

Fig. 2 Sketch of an oblique accelerating double layer and of its surrounding region [21]



in the downward current region where electrons of ionospheric origin are accelerated upwards.

2.2.1 How do large amplitude strongly localized parallel electric fields form and evolve?

Stationary models of DL and FAST data suggest that DLs propagate along magnetic field lines at the ion-acoustic speed, which is of the order of 10 to 50 km/s in auroral regions. The amplitude of the potential step along the field-lines is inferred from 3D electric field data. However these single point measurements cannot explain how double layers form and evolve and they cannot tell us whether the lifetime of these structures can account for the quasi-stationary nature of auroral forms that are believed to be associated with them. Numerical simulations suggest that DLs form in 1D current-driven plasmas in the presence of density fluctuations [18]. However, they might be destabilized by their interaction with nonlinear ion structures emerging from the interaction of the accelerated ion beam with thermal plasma after $\sim 500 \omega_{pi}^{-1}$, which corresponds to ~ 1 s in the auroral regions [19]. This non-stationarity would mean that parallel acceleration by a single strong DL cannot account for the quasi-stationary nature of inverted-V auroral arcs.

During the parallel phase of the mission, we will be able to detect DLs at two different altitudes, to observe their time evolution, and to check for the stationarity of individual DLs. The time delay for observing the structure by the two spacecraft should vary from a fraction of its expected lifetime (~ 1 s) to a few times this number. Separation distances of 10 to 100 km are required to answer these questions. An auroral imager with <10 s time resolution is needed to follow the evolution of the 10–50 km scale arcs associated with quasi-stationary field-aligned currents.

2.2.2 What is the vertical structure of Auroral Accelerating Regions (AAR)?

Large scale models of the vertical structure of AAR [20] show that the magnetic mirror effect and the anomalous resistivity due to wave turbulence triggered by field aligned current might contribute to maintain small amplitude quasi-stationary potential drops along auroral field-lines. However numerical simulations taking into account the interaction between magnetospheric and ionospheric plasmas show how strong DLs can play a key role [21]. Most of the electric potential drop along the field-lines was found to be concentrated in two layers. While the low-altitude transition layer of this model would correspond to the strong DL observed by FAST, the auroral cavity would be bounded at higher altitude by a second transition layer, with a large potential drop (several kV). Can we observe this high-altitude ion transition layer? Or is there a more complex pattern of multiple transition/double layers that would simultaneously exist? Are these stationary structures? If not, is there some kind of fast reformation mechanism of the structures that would maintain a constant time-averaged accelerating potential along the auroral field-lines?

Measurements at two altitudes will quantitatively constrain the large scale models of AAR by providing information about the distribution of particle distributions and electric fields. In the case of unstable layers, it will be possible to identify reformation mechanisms. We will be able to test the current–voltage relationship [22] that plays a key role in these models. Inter-spacecraft separation distances from 50 to 500 km are required to answer these science questions. The main required measurements are dc electric field, high-time resolution electron pitch-angle, and 3D ion distributions together with auroral imager data in order to follow the evolution of the 10–50 km scale arcs that are believed to be associated with quasi-stationary magnetic field-aligned currents.

2.2.3 What are the properties of ion hole turbulence in the upward current region?

In the upward current region, above the low-altitude DL, accelerated ionospheric ions drift at different speeds due to their mass differences, whereby multi-stream plasma instabilities can develop in the auroral cavity. The FAST satellite has measured ion cyclotron waves and nonlinear waves dubbed ion solitary waves [23]. The latter have propagation speeds in the hundreds of km/s, typically the order of the ion beams, and are characterized by a bipolar electric signal along the magnetic field with duration of 10 ms. They are usually referred to as ion holes.

Theory and simulations have shown that ion holes can form in the cavity 50 km above its bottom. They result from the spatial growth of electrostatic waves destabilized by the two-stream instability between the beams of H^+ and O^+ [24]. They propagate with a speed on the order of 200 km/s which is bracketed by that of the slow O^+ beam and the faster H^+ beam. From FAST measurements it was concluded that the ion holes observed had a speed larger than the H^+ beam. However only the electric field intensity and the time the structure takes to transit by the satellite was directly measured. Its amplitude was indirectly estimated by evaluating the response of the electron spectrum. From this estimate, the size and finally the speed of the structure was obtained. Dual satellite measurements will provide a direct measure of the speed of ion holes by estimating the delay of the electric field signature between the spacecraft. Spacecraft distances from 10 to 100 km are needed, corresponding to time delays <1 s over which ion holes are expected to be stable.

It is also known that O^+ ions have a larger pitch-angle than H^+ ions in these regions. This is either due to the non-adiabatic motion of O^+ ions that cross the low-altitude DL or by the selective perpendicular heating of low charge/mass ratio ions by ion-cyclotron turbulence. During the parallel phase, we will be able to discriminate between the two models, since one mechanism occurs at the transition layer itself while the other occurs 50–100 km above. A spacecraft separation distance less than 200 km is needed in order to simultaneously monitor the transition layer and the region where ion holes and ion cyclotron turbulence develop. To address this topic, it is necessary to measure dc electric

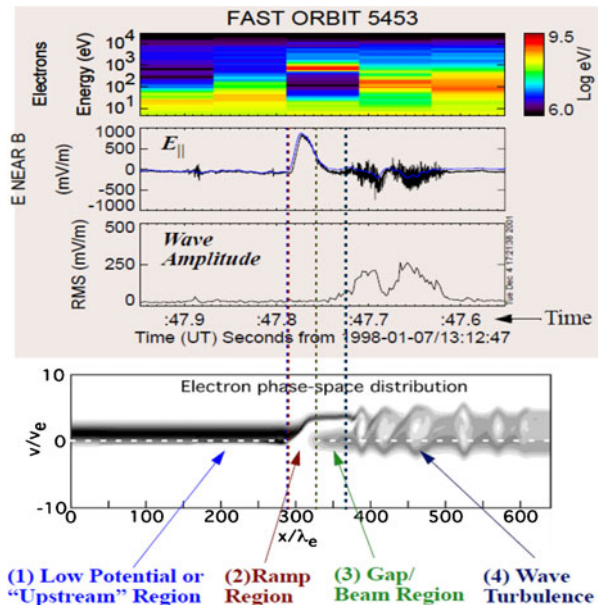
field and ULF/ELF waves and 3D ion distribution with mass discrimination capabilities.

2.2.4 What are the properties of electron hole turbulence in the downward current region?

In the downward current region (Fig. 3), strong DLs are associated with a strong plasma turbulence composed of fast moving, large amplitude, Debye scale length, 3D electric field structures that have been interpreted as electron phase space holes [25]. They are generated by electron beam plasma interactions downstream of the accelerating DL. Their velocity has been estimated by interpreting their magnetic signature as due to the Lorentz transformation in the spacecraft reference frame of a purely electrostatic structure. However in weakly magnetized plasmas, recent observations by THEMIS and CLUSTER spacecraft have shown that electron holes can have a proper electromagnetic signature. Alfvén will investigate the nature (electrostatic vs. electromagnetic) of electron holes and their velocity in the strongly magnetized auroral zones. Dual spacecraft measurements will give a direct estimate of their velocity. It will then be possible to derive their spatial size and amplitude, and to check the consistency of 3D electron hole models.

3D numerical simulations have shown the decay of 1D electron holes and the simultaneous emission of lower-hybrid waves while stability analysis of 3D electron holes suggests that a bounce resonance between trapped electrons and

Fig. 3 FAST observations of DLs and wave turbulence, and numerical simulations [19]

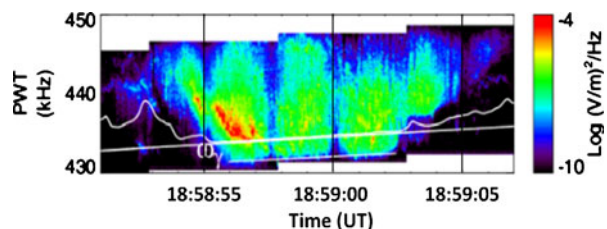


electrostatic whistler waves (from lower-hybrid up to plasma frequency) might take place [26], which would reduce electron hole lifetimes. Since electron holes have been frequently observed in association with bursts of Very Low Frequency waves [27], electron holes might eventually dissipate by emitting these waves (VLF saucers). During both parallel and transverse phases of the mission, the spacecraft will cross the source region of VLF saucers and at the same time they will observe the development of electron holes which will allow us to understand how this strong plasma turbulence dissipates.

2.3 The auroral kilometric radiation

The very first satellites that carried radio receivers made the surprising discovery that Earth is an intense radio source. This Auroral Kilometric Radiation (AKR) extends from 50 kHz to 700 kHz. It is generated between 2,000 and 12,000 km altitude with a peak power at $\sim 5,000$ km. AKR, so named because at 300 kHz it has a 1 km wavelength in free space, is usually not detected on the ground because of shielding by the ionosphere. The total AKR peak power levels can be as high as 10^9 W during strong substorms, corresponding to several percent of the total substorm energy. Viking and FAST satellite observations [28] have shown that the emissions occur slightly below the local gyrofrequency in regions of highly diluted plasma that contain earthward accelerated hot electrons (see Fig. 4). A Cyclotron Maser Instability (CMI) [29] occurs when electrons gyrating around the magnetic field resonate with the background of EM waves. In the dilute auroral cavity, even weakly relativistic non-Maxwellian electrons may invert the absorption coefficient of EM waves in the plasma which radiates in concert like a maser and emits intense coherent radiation. CMI is most efficient when the distribution of electron perpendicular velocities presents a positive gradient over a significant fraction of the resonance curve [30]. FAST satellite data showed that parallel electric fields in cooperation with the magnetic mirror force lift the electron distribution into an excited level by generating a ring or horseshoe distribution with a strong perpendicular gradient. The radiation is emitted primarily in the Right hand polarized extraordinary (RX)-mode at the local relativistic electron gyrofrequency into a strictly perpendicular direction with respect to the magnetic field [31].

Fig. 4 AKR FAST spectrum. The *bold white line* shows the electron gyrofrequency. The *thin white line* shows the expected AKR cutoff [28]

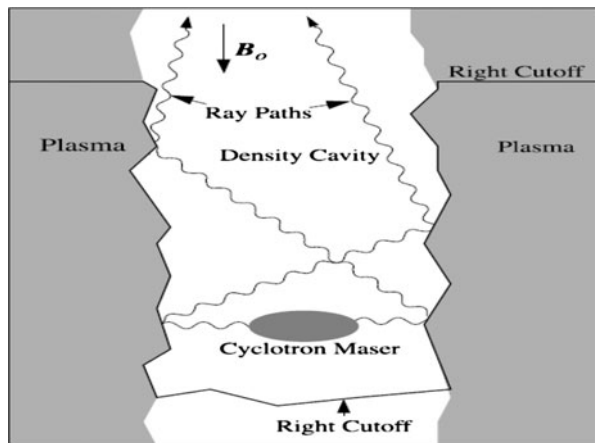


2.3.1 How does the radiation escape?

It is not understood however how the radiation escapes from the local density cavities where it is generated. The AKR source region lies within a density cavity bounded by a region containing a much denser thermal population (see Fig. 5). The perpendicular (to the magnetic field) dimension of the AKR source is typically ~ 100 km. The source region emissions are generated in the RX-mode, above the RX cutoff frequency which is an increasing function of the density and the magnetic field strength. Thus the density gradient at the edges of the cavity will reflect the radio waves, and in addition, earthward propagating emissions will also reflect due to the increasing magnetic field strength nearer the Earth.

There are several possible windows of escape: for example, mode conversion to the R-mode which has a nearly parallel propagation with a small optical depth along the magnetic field, or alternatively, partial or total mode conversion at the dense plasma walls boundary into either the Z mode or the L-O mode. These modes have different polarization patterns. The CMI mechanism itself is expected to produce strongly elliptically polarized waves that shall consequently be observed at least within AKR sources. From outside of the cavities, AKR has been observed to display quasi-purely circular polarization [32] with a possible small parallel component [33]. The Alfvén spacecraft will measure the complete AKR polarization state. With two spacecraft at 10 to 100 km separation distance and at different oblique angles relative to the static magnetic field, it will be possible to understand how mode conversion works. Poynting flux estimates will be essential to quantify the efficiency of the conversion mechanisms, to understand polarization transfers along the ray path and which information is carried by the radio waves reaching free space.

Fig. 5 Ray paths of AKR escaping from the auroral cavity [31]



2.3.2 What generates the AKR fine structure?

The second unresolved problem is the enormous fine structuring of the radiation as illustrated in Fig. 6. The spectral resolution of the AKR emission strongly suggests that a large part of the emission is made up of narrowband (down to less than 100 Hz) drifting structures. Often, the central frequency of the individual emissions varies in a systematic manner, sweeping either upward or downward across the spectrum. As AKR emissions take place near the electron cyclotron frequency, earthward (anti-earthward) drifts in space are reflected by upward (downward) drifts in frequency-time diagrams. Assuming a dipole magnetic field geometry, a bandwidth $\Delta f \sim 100$ Hz corresponds to ~ 1 km for the radial size Δz of the elementary radiation structures. The speeds of the elementary radiators can be derived from the measurement of their instantaneous df/dt ; according to their bandwidth they are quite variable and range from the ion acoustic velocity to the electron thermal velocity.

The simplest assumption is to identify the emission sources with real, drifting small-scale (1 km corresponding to several Debye lengths) physical objects. It has been speculated that electron [34] or ion [35] phase-space holes associated with double layers as well as double layers themselves [36] might play a key role in generating different AKR fine structures: the parallel electric field they carry would locally modify the electron distribution function and would enhance the radiation. However, simultaneous measurements by

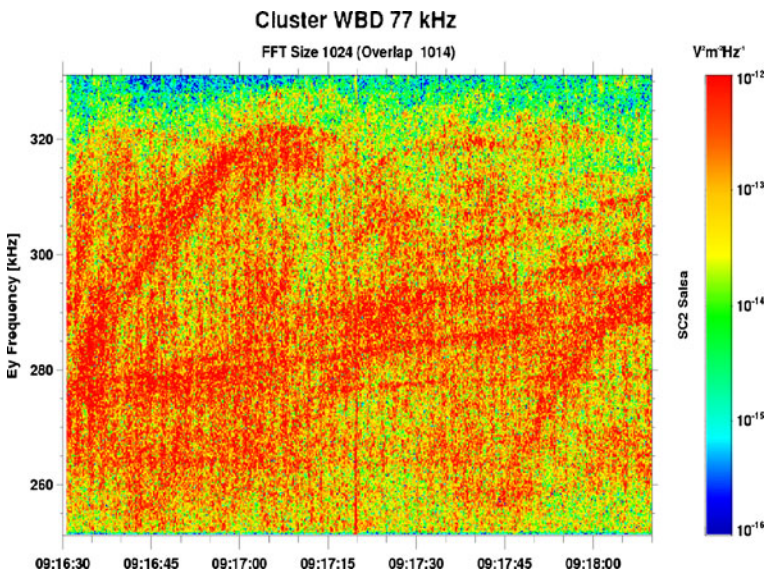


Fig. 6 Cluster observations of AKR fine structure (courtesy of J. Pickett University of Iowa, USA)

two satellites crossing the AKR source region at two different altitudes are required to validate this scenario. Two satellites located a small distance apart along the same magnetic field lines (or close by) crossing an AKR source region at the same time will measure the AKR frequency structures together with the characteristics (scales and velocities) of any turbulent nonlinear structures moving along the magnetic field lines, enabling a test of the scenario.

The possibility of a relationship between Alfvén waves and the generation of such AKR fine structure must be investigated as well. An Alfvén wave process is believed to play a role in the origin of some of the brightest short-burst Jovian radio emissions [37]. Fine structure in AKR emissions has also been observed at Earth in Alfvénic auroral acceleration regions between 2,500 and 3,600 km [38]. With the two Alfvén spacecraft, it will be possible to investigate the generation of AKR short bursts by Alfvén wave accelerated electrons, with one spacecraft crossing the source region while the other is observing the escaping radiation.

2.3.3 *Towards astrophysical applications*

The AKR source regions are identical to the auroral particle acceleration regions, implying that AKR is the only auroral phenomenon that provides remote information about the vertical structure and dynamics of the acceleration region. For instance, AKR has been used to characterize the two step-evolution of auroral acceleration at substorm onset [16]. Most of the information we have about acceleration/heating processes comes from the radiation emitted by astrophysical objects over a wide range of wavelengths. The AKR from the Earth can be taken as the paradigm for other manifestations of intense radio emissions.

The application of the CMI concept has been very efficient for explaining radiation from Jupiter and from other solar system magnetized planets [39]. The first crossings of the SKR source region at Saturn [40] display very close similarities with the terrestrial AKR counterpart, with some evidence of shell-like electron distributions. Another interesting similarity is that Saturn's SKR also exhibits a dual source character which might be linked to magnetotail reconnection and plasmoid/substorm evolution [41]. These results demonstrate that parallel acceleration and CMI generation processes do not only occur at Earth. Advances in studies of these phenomena at Earth will be applied in order to remotely probe the auroral regions of other magnetized planets.

More generally, the mechanisms may be active at magnetized planets, magnetic stars, flare stars, pulsars, and active galactic nuclei or blazars [42]. Speculations about radiation emitted from sufficiently strongly magnetized extra-solar planets have been published [43]. Scaling laws have been derived from solar system planetary radio emissions that relate the emitted radio power to the power dissipated in the various corresponding flow–obstacle interactions. Extrapolating these scaling laws to the case of exoplanets, it has been suggested that hot Jupiters may produce very intense radio emissions due to either magnetospheric interaction with a strong stellar wind or to

unipolar interaction between the planet and a magnetic star. Radiation of this kind, because it would be much stronger than any other radio emission, would allow not only allow detection of “radio-loud” extra-solar planets but also the inference of their magnetic field strengths and plasma properties. Because of its unique measurement capabilities, Alfvén will bring an improved understanding of AKR, which is needed if AKR is to become a reliable tool to probe astrophysical objects and, for example, to detect and/or characterize extra-solar planets.

2.4 Ionospheric ion outflows

The magnetosphere of the Earth has two plasma sources, the solar wind/magnetosheath at the outer boundary and the ionosphere at the inner boundary [44]. The auroral ionosphere is a particularly important source of plasma during magnetic storms, when heavy ions of ionospheric origin can become dominant in large parts of the magnetosphere [see e.g. 45]. The final fate of ionospheric ions is dependent both on the magnetic connection between the source region and the magnetosphere and on the typical energy of escaping ions. The large-scale impact of ion outflow also strongly depends on its mass flux. Cusp outflow is most likely to escape from the magnetosphere. Polar cap and polar cap boundary layer outflow is more likely to contribute to auroral dynamics and the development of auroral storms. None of these different source regions are uniform in space and time in the way they provide ionospheric material to the distant magnetosphere. Studies have shown a one - to - one relationship between poleward moving auroral forms (PMAFs) and ion upflow events in the auroral cusp, which indicates that the ion outflow phenomenon is driven by pulsed reconnection [46]. Ionospheric ion outflow can also induce the formation of low conductance regions which may affect the electrodynamics of the ionosphere-magnetosphere interaction. Finally ion outflow, in particular from the cusp and polar cap, is important from a planetology point of view, as this outflow may be lost from the atmosphere and thus affect atmospheric evolution on the long term [47].

2.4.1 *What is the spatio-temporal variability of ion extraction mechanisms?*

The amount of ion outflow is critically dependent on the source altitude of the outflowing plasma. The richest source is typically the ionospheric F region, located at an altitude of typically 300–500 km. It consists mostly of O⁺. Processes that can extract plasma from the ionospheric F region or below are most effective in locally removing O⁺ ions. They can lead to very low ionospheric densities which, if the E region is also affected, can lead to conductance structures which will affect the auroral electrodynamics. The initial upflow of plasma from the F region can be studied by radars like the EISCAT facility but so far they only provided altitude profiles from one point [48].

Two perpendicularly separated spacecraft will for the first time allow us to measure the spatial scales over which the extraction mechanisms operate, and

separate this from the time scales for intermittent extraction. The initial upflow results from Joule heating in the ionosphere and from enhanced ambipolar diffusion caused by elevated electron temperatures which in turn are caused by (mainly soft) electron precipitation [49]. If there is no further energisation of the ions at higher altitude the ions will fall down into the ionosphere again. Even a little heating, well below what is needed to reach escape velocity, may stop the ions from returning to the ionosphere due to the effect of the mirror force. Ions may thus stay in an intermediate region until they are heated enough to overcome gravity [50].

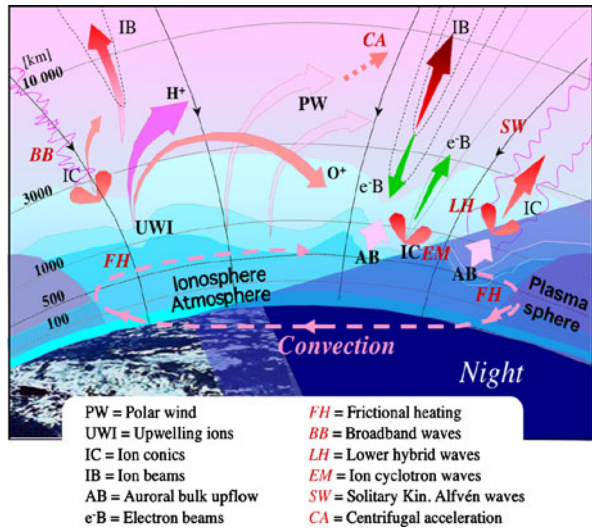
Two spacecraft separated in the perpendicular direction will allow us to study the spatial scales and persistence of such waves, as well as the drift of gravitationally bounded ions which are kept from returning to the ionosphere through the mirror force of the magnetic field. Systematic measurements by spacecraft aligned along the field-line will show if the waves are typically present over large distances along the field-line or if they only exist in narrow regions. Ions may also be trapped by downward directed field-aligned electric fields, not just gravity, or be heated in the parallel direction. Perpendicularly separated spacecraft will show how these conics evolve with time, whereas altitude separated spacecraft can show how they evolve along the field-line.

2.4.2 How efficient are the various ion energisation mechanisms?

Throughout the outflow path the ions may be subject to heating and acceleration. In the main auroral oval direct acceleration by parallel electric fields is expected to be an important driver in the nightside and in the afternoon sector. However, wave particle interaction leading to transverse heating is expected to be the most important mechanism at low altitude and over extended altitude intervals in the dayside cusp/cleft and in the polar cap boundary layer in the nightside. Among the many energisation mechanisms depicted on Fig. 7, Alfvén wave turbulence, that often takes the form of broadband ELF waves, has been studied by e.g. Chaston et al. [51]. It is a good candidate for the formation of regions of depleted plasma. However, it is also well-known that the presence of background field-aligned currents (which are themselves related to the dynamics of the aurora) affect the presence of ion cyclotron waves which can directly heat ions through a resonant process. FAST measurements show that the electron beam drives electrostatic ion cyclotron waves both in upgoing ion and upgoing electron beams [52]. Heating may also occur in association with density cavities, in particular lower hybrid cavities, low density regions which are filled with intense lower hybrid waves [53]. Another acceleration mechanism which is important at least for cusp and polar cap ion outflow is the centrifugal acceleration mechanism that has been studied with the Cluster spacecraft at high altitude [54]. Finally oblique field-aligned electric fields, as already described in Section 2, might also be important in regions of strong field-aligned currents.

A two spacecraft mission with varying perpendicular separation will allow us to study for the first time the structuring of both waves and particles at different

Fig. 7 Summary of ionospheric ion outflow related processes [44]



spatial scales, thus allowing us to characterize and understand the turbulence that is related to ion heating. We will be able to systematically probe the scale size and lifetime of associated cavities and of field-aligned current regions. We will observe how associated electric fields and ion distribution functions evolve in and around the cavity/field-aligned currents. Altitude separated spacecraft will allow us to study the propagation of waves and turbulence along the field lines. These measurements will constrain the numerical models that integrate along magnetic field-lines the cumulative effect of specific energisation mechanisms and we will be able to assess their relative efficiency. Mass resolved measurements will be most important to distinguish between these different acceleration mechanisms since many of them are mass dependent. Such processes occur at all planets where ion outflow has been detected, but only at Earth is it likely that we will ever have the multi-point measurements appropriate to study the mechanisms leading to ion heating and outflow.

3 Mission profile

3.1 Introduction

The minimum requirement in order to meet the science goals discussed here is for a well instrumented dual spacecraft mission, in which the spacecraft separation is varied along and across the magnetic field for selected length scales, covering the range of altitudes at which auroral particle acceleration occurs. During the preparation of the concept proposed to ESA, an alternative three spacecraft mission concept was also developed. The three spacecraft mission offered advantages such as the possibility of simultaneous measurements of

perpendicular and parallel scales, and less severe reduction in science return in the event of instrument or even spacecraft failure. The three spacecraft mission was also more expensive and while it was not expected to exceed the mission cost cap, the team choose to propose the two spacecraft variant which is discussed in detail in this paper.

3.2 Orbit requirements

3.2.1 Operational orbits

The scientific aims of the mission require that dual-spacecraft operations are performed over the range of altitudes and magnetic latitudes where the auroral acceleration region is located. Coverage of all magnetic local times is required, although a subset is of prime interest for studies of the substorm onset region in the pre-midnight MLT sector, and of the cusps on the dayside centred on noon MLT. For science planning purposes, we referred to a statistical study of the probability of observing accelerated auroral electrons with energy flux $>0.25 \text{ erg cm}^{-2} \text{ s}^{-1}$ for all IMF conditions [55] and in particular an improved quality figure based on that study [56]. The region of maximum probability is within the ranges; ILAT $65^\circ\text{--}75^\circ$, MLT 20–22 h; and a wider region of high probability is within the ranges; ILAT $70^\circ\text{--}80^\circ$, MLT 12–18 h; ILAT $65^\circ\text{--}75^\circ$, MLT 18–24 h.

We present one possible orbit strategy that we have developed, with some assistance from CNES and Astrium. We note that more detailed follow-on studies might well result in a better optimised approach.

- Initial orbit: 500 km circular polar orbit. This is used for commissioning and as a parking orbit before transition to the main operational orbits, improving launch date flexibility.
- Reference Orbit 1 (RO1): 500 km \times 4,000 km elliptical polar orbit, (similar, but not identical to the orbit of the FAST spacecraft).
- Reference Orbit 2 (RO2): 500 km \times 8,000 km elliptical polar orbit.
- De-orbit phase: reduce perigee to 250 km, atmospheric drag gradually causes deorbit.

In Table 1 we summarise strawman parameters for the main science mission. For simplicity we set the spacecraft transition to RO1 to occur on the autumn

Table 1 Summary of the strawman mission design parameters

| Orbit phase | Perigee \times apogee (km) | Orbit period | Line of apsides rotation period (days) | Mission phase start (d/m/y) | Phase duration (days) |
|---------------|------------------------------------|--------------|--|-----------------------------------|-----------------------------|
| Initial orbit | 500 \times 500 | 1 h 34 m | n/a | flexible | flexible |
| Ref. Orbit 1 | 500 \times 4,000 | 2 h 13 m | 192 | 22/09/20 | 780 |
| Ref. Orbit 2 | 500 \times 8,000 | 3 h 02 m | 331 | 10/11/22 | 721 |
| De-orbiting | 250 \times 8,000 | 2 h 58 m | tbc | 09/11/24 | tbc |

equinox, at which time the orbit plane is required to lie in the noon-midnight meridian. The plane of the RO1 polar orbit is fixed in inertial space and will rotate about the Earth once per year (similar to Cluster or Double Star TC-2). The line of apsides of the RO1 orbit will rotate around within its orbit plane once in 192 days. We wish to achieve magnetic conjunctions with the region of highest probability of observing accelerated auroral electrons while at apogee in northern hemisphere winter months, to favour co-operation with ground based optical observatories. We determined that to achieve this, the argument of perigee of the initial RO1 orbit should be 192° on 22 September. Similarly, the transition to RO2 which should ensure that conjunctions continue to occur over that region as the mission progresses, and we chose a transition date of 10 November 2022 at which point the argument of perigee (in both RO1 and RO2) is 290° . In Table 1 we summarise the mission orbits and timeline, and indicate an arbitrarily selected date to end the RO2 phase after 2 years.

Figure 8 shows that there are 4 intervals with conjunctions in the 18–24 MLT sector in the northern hemisphere in the 2 years of the RO1 orbit. There are 2 more while in the RO2 orbit together with 2 intervals in the 12–18 MLT sector. There are also a similar number of southern hemisphere intervals which are equally useful for in situ measurements, but which will be less well supported by ground-based facilities. Since the period of rotation of the line of apsides is

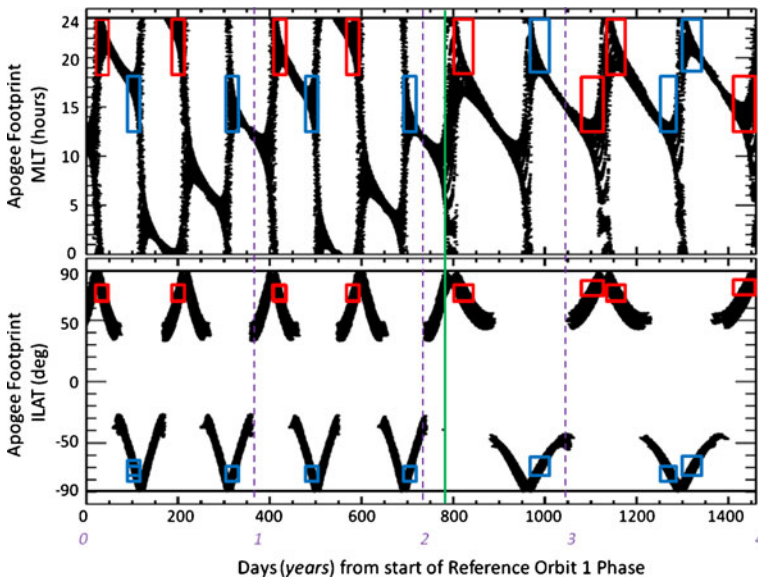


Fig. 8 Magnetic footprint coverage for times when the spacecraft are at apogee, for 4 years of science operations. The *green line* at day 780 marks the transition from Ref Orbit 1 to Ref. Orbit 2. *Red (blue)* boxes show intervals of good coverage in the northern (southern) hemisphere for the MLT/ILAT regions with the highest probability of seeing accelerated auroral electrons. Cusp observations are possible near 12 MLT at similar latitudes to those of the auroral observations

not an integer fraction of 1 year in either RO1 or RO2, the coverage pattern of the auroral oval changes as the mission proceeds, as indicated in Fig. 8 (this is an area where further optimisation may be possible). The distribution in time and in ILAT/MLT of useful magnetic conjunctions while the spacecraft are in the AAR altitude range will be higher than shown in Fig. 8 since the plots concentrate on the apogee intervals and ignore time when the spacecraft are elsewhere on their orbits but are also within useful ILAT/MLT regions.

Figure 9 (upper panel) shows our estimates of the accumulated time spent with the spacecraft magnetic footprint in the auroral zone; the red line refers to the 12-18-24 MLT semi-oval, showing values of 1–2 h per day in RO1 and more in RO2. The black line refers to all MLTs, i.e. the complete auroral oval, and shows roughly double the accumulated time.

Significant additional scientific opportunities will arise by combining space measurements made by Alfvén with simultaneous conjugate observations of the aurora and of the detailed nature of the conjugate ionosphere made by ground observatories, particularly in Northern Europe and North America. Nordic infrastructure today [57] includes EISCAT, Super-DARN, MIRACLE (Magnetometers, Ionospheric radars, Allsky Cameras Large Experiment), ALIS (Auroral Large Imaging System) and ASK (Auroral Structure and Kinetics). Furthermore, funding has been awarded for the planning of future

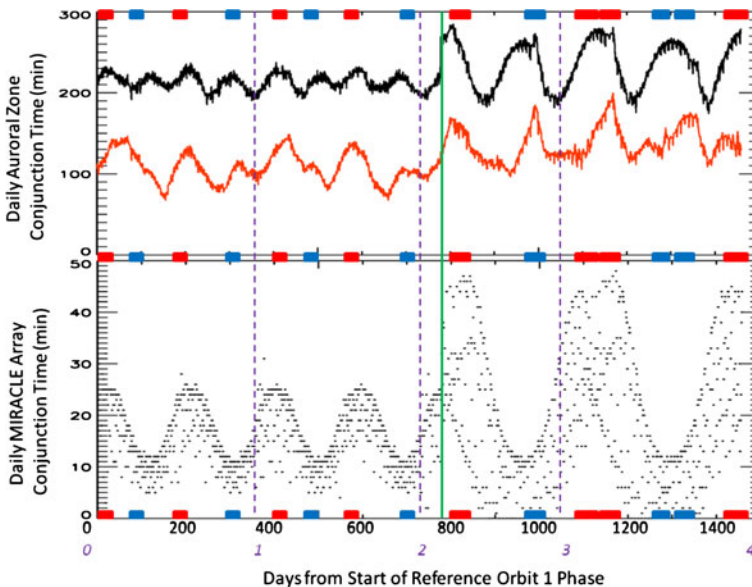


Fig. 9 Illustration of the daily accumulated time during which the spacecraft magnetic footprint is in the auroral zone (*upper panel*; red and black traces explained in the main text) or over the MIRACLE array (*lower panel*), for 4 years of science operations. As in Fig. 8, red and blue markers show the target intervals, which in general coincide with longer duration conjunctions, by design

capabilities in this region, specifically EISCAT_3D and SIOS (Svalbard Integrated Arctic Earth Observing System). As an indication of how often such observations will be possible, Fig. 9 (lower panel) shows the accumulated time spent with the spacecraft magnetic footprint above the Scandinavian MIRACLE network, which ranges between 5–25 min in RO1 and ranges up to 50 min in RO2. These values were determined with 1 min resolution orbit data and magnetic mapping using the current IGRF magnetic field model, accounting for the Earth's rotation, spin axis orientation and dipole tilt. There will be additional useful conjunctions with the network of ground-based facilities in North America but we do not assess those here.

The red and blue filled rectangles highlight the times at which the spacecraft conjunctions are in the regions of high probability of observing accelerated auroral electrons. It is clear from Fig. 9 that in the northern hemisphere (red rectangles) these coincide with the longer duration intervals of magnetic conjunctions with the auroral regions and intersections with the MIRACLE network, demonstrating that our mission design is reasonably effective.

The main science goals of the mission will be addressed with both spacecraft in each of the Reference Orbits, by varying the inter-spacecraft separation in two phases; a radial (parallel) separation phase (phase A) and a transverse separation phase (phase B). In our strawman mission outline, there are 2 years in each of RO1 and RO2; further study is required to determine the most appropriate division of the time between phase A and phase B operations, but the simplest approach is to share it equally.

3.2.2 Phase A: parallel spacecraft separations

A possible method of achieving suitable parallel separations is to modify the eccentricity of the orbit of one spacecraft without changing the semi-major axis. Differential drift of the argument of perigee produces a tilt between the lines of apsides of the orbits of the two spacecraft. The consequent radial spacecraft separation is indicated in Fig. 10. The process can be reversed on the same spacecraft, or executed on the second (which leads to more similar fuel usage on the two spacecraft) to stop the differential drift. It is more efficient to achieve the eccentricity change by decreasing perigee and raising apogee than vice versa. It is necessary to ensure that the two spacecraft are properly synchronised so that they arrive in the auroral region together, separated primarily along the magnetic field (\sim radially) without transverse separation. This can be achieved with proper planning as demonstrated by Cluster. The differential drift is relatively expensive in Δv and fuel. For example, the drift to 4° tilt would take ~ 3 months if using a Δv of 200 m/s. More fuel can achieve a given change more rapidly.

3.2.3 Phase B: transverse spacecraft separations

During this phase the spacecraft will be separated along the orbit track. A possible method is to temporarily alter the semi-major axis of one spacecraft,

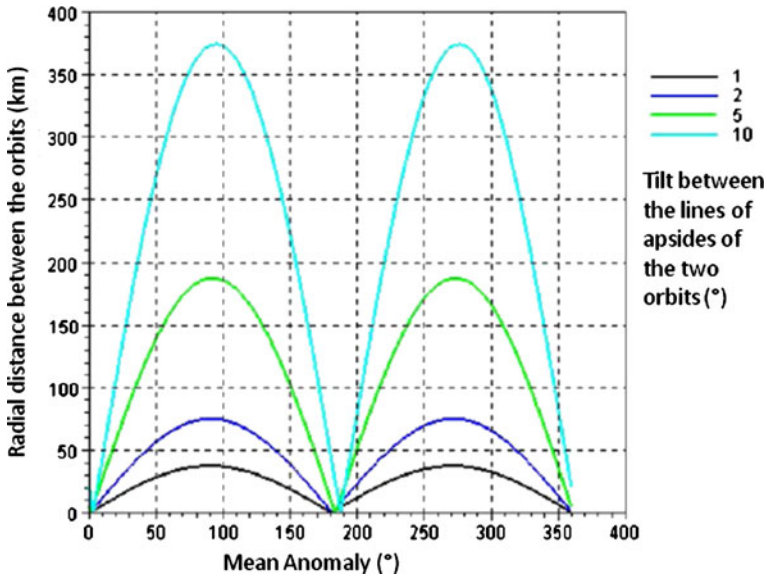


Fig. 10 Illustration of the variation with mean anomaly of the radial distance between two spacecraft on otherwise identical orbits, for which the angular separation of the lines of apsides are 1,2,5 or 10°

while preserving the eccentricity of its orbit. Small impulses at perigee and apogee can be used to achieve this, firstly to modify the orbit and then to return it to the original parameters. For small fuel costs (fractions of a kg, corresponding to $\Delta v < 1$ m/s), the spacecraft separation can be varied by up to 100 km scales within 1 day. Changes can be executed more quickly for larger fuel costs. In practice, a separation scale will be selected for a set of orbits before the scale is changed to another value and the process is repeated. The along track time delay for a 10 km separation at apogee is ~ 2 s, rising linearly to 20 s for a 100 km gap. We note that operations at comparable small separations have already been achieved during the ESA-NASA Cluster mission and will soon be demonstrated in the NASA Magnetospheric Multi-scale Mission.

3.3 Launcher and spacecraft manoeuvring requirements

3.3.1 Launch to initial orbit

The proposed launcher is Vega. The two Alfvén spacecraft can be launched from the Guiana Space Centre into an initial 90° inclination polar orbit of altitude 500 km. The Vega User Manual, (March 2006 version) indicates that the launch vehicle can deliver 1,623 kg to this orbit. We show below that the proposed spacecraft mass including fuel and 25% margin is of order 1,500 kg, and thus is well within the launch vehicle performance capability. Further

orbital changes can be performed with spacecraft onboard thrusters, following the example of Cluster.

3.3.2 Transfers to Reference Orbits 1 and 2

The feasibility of using Vega to launch two Alfvén spacecraft, each with adequate fuel to perform the mission phases outlined above, is shown in Table 2. The calculation is conservative as it assumes that all fuel needed for the Phase A and B operations (“Small Scale Manoeuvres”) is retained until the end of the mission, while in practice it would be used progressively during the mission. The specific impulse figures cover a range of values which includes the 280–290 s specific impulse of Cluster 10 N thrusters in pulsed or continuous mode and the 300 s recommend by Astrium for such thrusters. The 320 s case would be for a 400 N main engine as on Cluster, but not baselined for Alfvén, included for comparison. Astrium recommended that we consider 20% of the total fuel mass to be a good estimate of propulsion system mass (tanks, thrusters, associated structure). It is clear that after including a 20% system level margin, two spacecraft can be delivered to the planned 500 × 500 km altitude initial orbit by Vega. If for some reason Vega performance is in fact lower than expected at this stage of its development, our mission profile

Table 2 Demonstration that the spacecraft, payloads and fuel can be launched by Vega

| | | | |
|--|--------|--------|--------|
| Spacecraft details | | | |
| Engine specific impulse (s) | 270 | 300 | 320 |
| Dry mass excluding propulsion system h/w (kg) | 285 | 285 | 285 |
| Dry mass including propulsion system h/w (kg) | 343 | 340 | 339 |
| Fuel available for SSMs (kg) | 50 | 50 | 50 |
| Mass after LSMs, incl. SSMs fuel (kg) | 393 | 390 | 389 |
| Initial orbit | | | |
| Apogee altitude (km) | 500 | 500 | 500 |
| Inclination (deg) | 90 | 90 | 90 |
| Total mass Vega can deliver to this orbit (kg) | 1623 | 1623 | 1623 |
| Large scale maneuvers (LSMs) | | | |
| Ref. Orbit 1 apogee altitude (km) | 4000 | 4000 | 4000 |
| ΔV to apogee (km/s) | 0.7374 | 0.7374 | 0.7374 |
| Ref. Orbit 2 apogee altitude (km) | 8000 | 8000 | 8000 |
| ΔV to apogee (km/s) | 0.5119 | 0.5119 | 0.5119 |
| De-orbiting perigee altitude (km) | 250 | 250 | 250 |
| ΔV to perigee (km/s) | 0.0531 | 0.0531 | 0.0531 |
| Fuel and propulsion | | | |
| Total ΔV for LSMs (km/s) | 1.3024 | 1.3024 | 1.3024 |
| Fuel required for LSMs (kg) | 236.4 | 223.34 | 216.69 |
| Estimated propulsion system h/w [20% fuel] (kg) | 57.279 | 54.667 | 53.337 |
| Mass budget | | | |
| Spacecraft wet mass at launch (kg) | 629.4 | 613.34 | 605.69 |
| Spacecraft wet mass (kg) + ESA system margin @ 20% | 755.28 | 736 | 726.82 |
| Two spacecraft wet mass at launch (kg) | 1510.6 | 1472 | 1453.6 |
| Mass margin within Vega capability (kg) | 112.45 | 150.99 | 169.35 |

could be correspondingly adapted by lowering the apogees of the orbits, most likely without a major impact on the science.

3.3.3 Extended mission concepts

The nominal mission lifetime described here is 4 years. Significantly longer operations may be possible based on the experience of FAST in an orbit similar to RO1 (>10 years). Extended operations in any of the scientifically preferred configurations would be valuable, in order to improve statistics and coverage of the altitude range at all MLT.

An additional mission phase which could follow the RO2 phase would involve extending the differential drift of the line of apsides to 180° , allowing simultaneous imaging of the northern and southern hemispheres, and collection of related in situ data. This would provide the first opportunity to systematically study the effects of the different ionospheric illumination expected in the two hemispheres.

3.4 Ground segment requirements

As noted above, the line of apsides will rotate completely around the Earth, in about 6.5 months for RO1 and 11 months for RO2. In order to provide good ground station visibility while lingering near apogee, ground stations in both

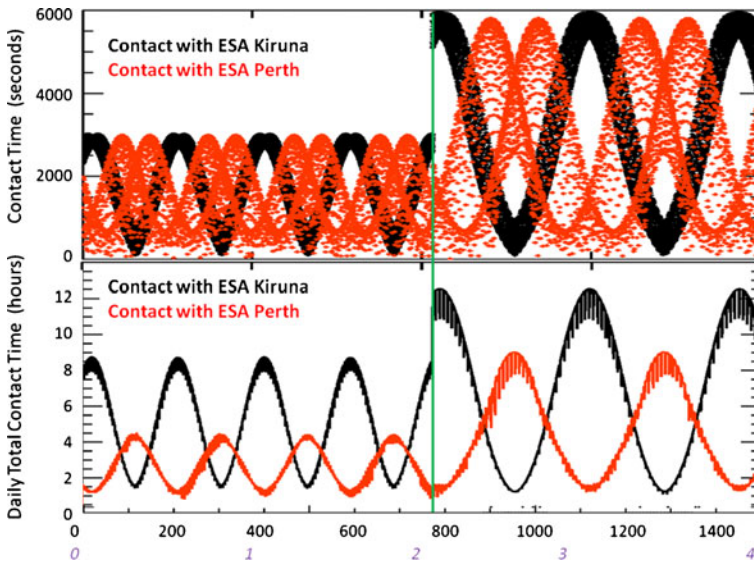


Fig. 11 Illustration of spacecraft-ground station access time, as the mission progresses. The *upper panel* shows the duration of contact times for each individual orbit, while the *lower panel* shows the accumulated daily total duration. Contacts with the northern hemisphere Kiruna station and the southern hemisphere Perth station are shown. It is clear that when one station has poor visibility of the spacecraft, the other can readily provide good coverage

the northern and southern hemispheres are required. Figure 11 shows that the daily average minimum contact time for the ESA Kiruna ground station is as low as 1 h, which can be improved to a minimum time of 4 h if support is also provided by the Perth ground station. It is clear that there are some individual orbits where contact time with a single ground station is very low, so the spacecraft would ideally have the capability to store data from more than one orbit between opportunities to transmit the data to a ground station. Alternatively, as proposed here it may be more cost effective to use a second ground station in the other hemisphere, to ensure that there are always contact intervals of a sufficiently long duration to transmit data from at least one orbit.

A preliminary study has demonstrated the feasibility of meeting the planned data return requirements using these ESA ground stations (for further discussion see Section 5).

4 Model payload

4.1 Overview of all proposed payload elements

Each spacecraft has an identical payload, consisting of a suite of Fields and Particles sensors together with a UV auroral imager. The payload is summarised in Table 3 and discussed in Section 4.3 below. For the purposes of the study, three Data Processing Units were described (for the Fields, Particles and Imager) since the resources required could be conveniently estimated based on

Table 3 Summary of the proposed Alfvén payload (mass and power excluding ESA margins)

| Payload element | Abbrev. | CBE | | TRL 2010 |
|---|----------|--------------|--------------|-------------|
| | | Mass/kg | Power/W | |
| Electric and magnetic fields; electromagnetic and electrostatic waves | | | | |
| Electric field: 3D | E3D | 7.40 | 1.83 | 8 |
| Magnetic field: 3D d.c. | MAG | 4.23 | 3.00 | 7 |
| Magnetic field: 3D a.c. (SC/MRM) | MADAM | 1.22 | 1.43 | 5 |
| Magnetic field: 3D HF loop | HFML | 4.55 | 0.64 | 6 |
| Current density (a.c.) loop/coil | CDC | 2.01 | 0.40 | 6 |
| Wave analysis (8 kHz–2 MHz) | AWI-HFR | 1.50 | 5.00 | 7 |
| Wave analysis (DC–16 kHz) | AWI-LFR | 0.45 | 3.20 | 5 |
| Radio sounder (electron density) | AWI-EDEN | 0.80 | 2.07 | 8 |
| Fields DPU | AWI-DPU | 2.80 | 6.79 | 6 |
| Plasma characteristics | | | | |
| Electron distributions: 2D (fast) | EESA | 6.90 | 5.40 | 5 |
| Ion distributions: 3D (fast) | IESA | 7.10 | 6.00 | 4 |
| Ion distributions: 3D (mass) | ICA | 1.90 | 6.43 | 7 |
| Multi needle Langmuir probes | MNLP | 4.28 | 3.40 | 6 |
| Particles DPU | PDP | 2.20 | 5.80 | 6 |
| Auroral Imaging | | | | |
| Wide Field Auroral Imager (UV) | WFAI | 3.56 | 10.51 | 5 |
| Imager DPU | IDPU | 1.80 | 6.15 | 5 |
| TOTALS | | 52.70 | 68.04 | |

previous work. A more detailed study may show that a combined unit could deliver the necessary functionality within a smaller resource allocation than for the three separate DPUs.

The mass of wire/stacer booms is included in E3D. The mass of the main rigid booms (4 m) is included in MAG and HFML respectively. The mass of the MNLP booms is included under MLNP. These mass and power totals may be compared with the corresponding values for the highly integrated payload of the smaller FAST spacecraft, which were 65 kg and 39 W.

4.2 Proposed payload accommodation

The suggested accommodation for the “fields” equipment is shown in Fig. 12. There are a pair of 40 m tip-to-tip electric field booms in the spin plane; a pair of 7 m tip-to-tip spin axis electric field stacer booms; two 4 m rigid booms to support the magnetometers, search coils, and loop systems. In addition, a pair of 0.7 m booms support the Langmuir needle probes; these are tilted out of the spin plane by $\sim 30^\circ$.

Figure 13 illustrates how the plasma instruments are mounted on a main experiment platform, looking out through the curved surface of the cylindrical spacecraft. The field of view of the plasma instruments are indicated in Fig. 13. Plasma and Imager Instruments should be aligned with the local spacecraft radius to within 15 arcseconds. Their field of view should be clear, with margin, and should not be affected by glint. The two EESA sensors should

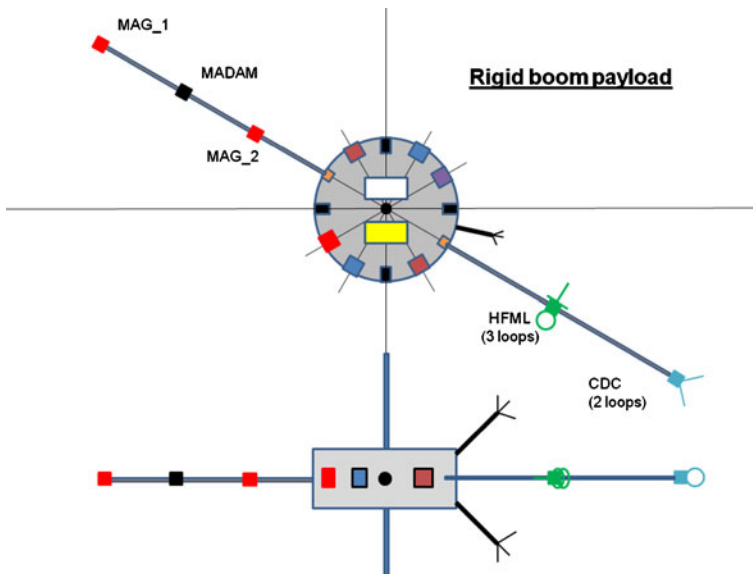


Fig. 12 Plan and elevation views of the spacecraft, illustrating the various booms and the accommodation of the “fields” sensors

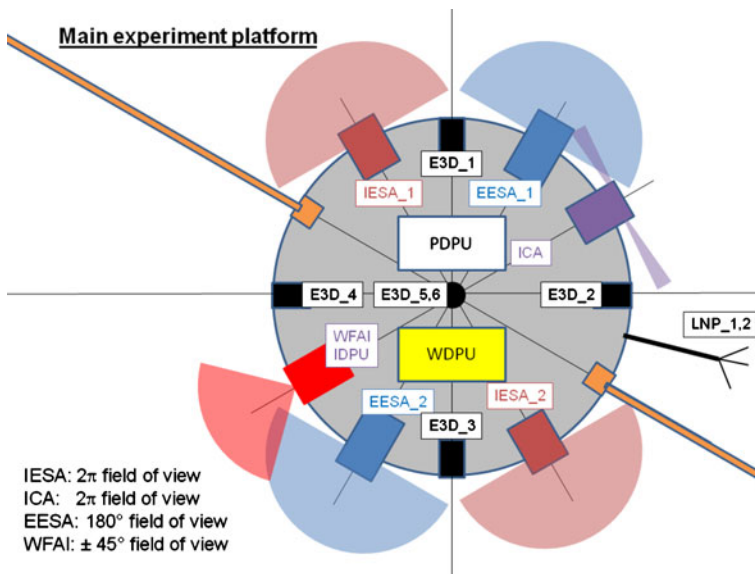


Fig. 13 Plan view of the spacecraft main experiment platform, illustrating the accommodation of the “particles” sensors, boom footings, auroral imager and data processing units

be diametrically opposite one another, so that their combined field of view is 360° in each case. Similarly for IESA.

4.3 Proposed instrument complement

4.3.1 Overview

The payload of the Alfvén mission and its accommodation on the spacecraft platform is fully adapted to the study of the AAR at high-time resolution. The Electron and Ion ElectroStatic Analyzer (EESA and IESA) provide a 2D pitch-angle distribution within 40 and 100 ms, respectively (compared to 2 to 4 s on Cluster). The 3D electric fields will be measured by E3D instead of 2D electric fields on Cluster, which is essential in order to study parallel electric fields.

Key magnetic field measurements are fully redundant with 2 MAG sensors, also allowing correction of any residual magnetic interference from the spacecraft. MAG and MADAM observations have some overlap and will be cross-calibrated. HFML provides a 3D measure of high-frequency magnetic waves (there was no measurement of this type on Cluster), which is most important for AKR studies. CDC will for the first time partially solve the basic spatio-temporal ambiguity between small-scale (typically between 10 m and 5 km) current structures and dispersive Alfvén waves. The High Frequency Receiver (HFR) will continuously provide the complete spectral matrix of electromagnetic waves which will be a first at high frequency in the AAR and

a key measurement to understand how AKR escapes from the AAR and to quantify this process.

All instruments are at Technology Readiness Level (TRL) 5 or higher at the time of writing, with the exception of IESA which is in development and expected to reach TRL 5 by spring 2012. Most instruments have spaceflight heritage, often from multiple missions, and use technologies that are well established in Europe.

All instruments will have a standby mode (reduced power but ready to quickly begin science measurements) and one or more (but few) science operations modes. Options for internal calibration modes or engineering modes are anticipated. Some instruments may need specific commanding when the system shifts from slow survey to fast survey to burst mode.

All instruments will undergo appropriate ground calibration. In-flight inter-calibration of instruments will be carried out using routinely acquired datasets.

4.3.2 3D electric field

The E3D electric field experiment provides rapid measurements of 3D electric field to an accuracy of 1 mV/m on the two spin plane components and 10 mV/m on the spin axis component, up to a limit of 1 V/m. It also provides an estimate of spacecraft potential up to 50 V. The technique involves measuring the probe-spacecraft potential differences on pairs of probes on opposite sides of the spacecraft. In addition to measuring slowly varying local electric fields, electric components of electrostatic and electromagnetic waves of frequencies up to a few MHz can be measured and are received and processed by other experiments (the Low and High frequency Receivers). The 20 m long spin plane wire booms are deployed from units mounted on the main experiment platform. The spin axis stacer booms are shorter (3.5 m long) in order to minimise disturbance to spacecraft attitude stability. Sensors and preamplifiers are placed at the ends of the booms.

4.3.3 Magnetic field: MAG

The MAG magnetic field experiment provides rapid measurements of the 3D magnetic field vector in the bandwidth DC to 64 Hz in fields as strong as 65,000 nT. Instrument accuracy is of order 0.1 nT, but the practical resolution of the measurements is sized in proportion to the measured field intensity due to the digitalization of the signal. With 16 bit data words, it would be 2 nT. The planned rate of science data is 16 vectors/second. The technique is the widely used fluxgate method. The instrument consists of two tri-axial fluxgate magnetic field sensors, mounted at different distances along one of the rigid booms to allow identification and correction for any unexpected magnetic interference from the spacecraft. The magnetometer alignment must be stable and known to an accuracy better than 0.1° , translating to a requirement for a rigid boom and spacecraft attitude knowledge known to better than 0.1° .

4.3.4 Magnetic field: MADAM

Disturbances to the magnetic field in the frequency range 0.1 Hz to 25 kHz will be measured by the MADAM instrument, which also measures the magnetic field from quasi-DC to a few Hz with an auxiliary sensor. The main sensor is a magnetic field search coil which consists of tri-axial loop sensors, and the auxiliary sensor is a miniature magnetoresistive sensor which is incorporated into the search coil mount. The magnetic field strength resolution is ± 10 nT in the flat part of the search-coil transfer function from 100 Hz to 10 kHz and 20 dB/decade higher outside the flat part, and ± 0.1 nT for the auxiliary sensor. The instrument sensitivity can be expressed in terms of equivalent input magnetic noise levels as low as: <20 pT/ $\sqrt{\text{Hz}}$ at 1 Hz, 2 pT/ $\sqrt{\text{Hz}}$ at 10 Hz, 0.2 pT/ $\sqrt{\text{Hz}}$ at 100 Hz, 0.025 pT/ $\sqrt{\text{Hz}}$ at 1 kHz. The instrument is designed to ensure that the maximum magnetic field at the spin frequency does not saturate the search coil output. The sensor must be mounted on a rigid boom, at least 1 m from the spacecraft. Adequate separation from other boom payloads should also be provided. Supporting analog electronics may be mounted with the sensors on the boom, or at the foot of the boom.

4.3.5 Magnetic field: HFML

Disturbances to the magnetic field in the frequency range 20 kHz to 2 MHz will be measured by the High Frequency Magnetic Loop instrument [58], which thus complements the search coils. HFML uses 3 loops of diameter 20 cm each, and provides measurements of all three magnetic components, similar to the search coil. The instrument will measure Auroral Kilometric Radiation emissions, which have peak intensity in the 100's kHz range. Instrument bandwidth is 3 dB and sensitivity is 0.3×10^{-6} nT/ $\sqrt{\text{Hz}}$ at 1 MHz for a 20 cm diameter coil. The sensor and associated analog electronics must be mounted on a rigid boom at least 1 m from the spacecraft to minimise spacecraft electromagnetic interference.

4.3.6 Electric current density: CDC

The varying current density in the ELF frequency range can be directly measured by a Current Density Coil sensor [59]. The sensor consists of a 15 cm diameter toroidal coil with primary and secondary windings, and the measured quantity is AC current flowing through the loop. The technique is based on Ampère's Law. Taking account of spacecraft motion, this will reveal changes in current density (in a specific direction) as the spacecraft crosses field aligned current layers, even double layers, associated with auroral arcs. By comparing measurements from the 2 spacecraft during the transverse phase, it will be possible to identify the proper motion of small-scale current structures. It will enable the distinction between small-scale current structures and Alfvén waves. The bandwidth is 3 dB (1 Hz–450 Hz) and sensitivity is 0.3×10^{-6} A m $^{-2}$ / $\sqrt{\text{Hz}}$ at 10 Hz and 1.0×10^{-6} A m $^{-2}$ / $\sqrt{\text{Hz}}$ at 1 Hz. The sensor and

associated analog electronics must be mounted on a rigid boom at least 2 m from the spacecraft to minimise spacecraft electromagnetic interference.

4.3.7 *Electromagnetic wave signal processing unit and sounder: AWI*

The main function of the Alfvén Wave Instrument is to digitize analog signals from the 3 fields and waves instruments HFML, E3D, and MADAM, to calculate Fourier spectra of the signals and to prepare data products that can be passed to the Fields DPU for downlink or on-board storage. It also contains an active sounder that excites plasma resonances in order to probe the absolute value of the electron plasma density. Internally, AWI is composed of three hardware modules that would share a common electronic box:

- HFR** The High Frequency Receiver will provide unique information about electromagnetic radiation in space plasmas by performing, for the first time, a complete goniopolarimetric study of Auroral Kilometric Radiation and other emissions like VLF saucers. The HFR performs duty cycled snapshot digitization of one of the electric and magnetic signals from the HFML or E3D instruments. It calculates the power spectra of 5 of the electric and magnetic signals in the frequency range between 8 kHz and 2 MHz together with their cross-spectra from which information about k -vector, polarization, and Poynting flux can be derived.
- EDEN** The electron density will be measured at high altitudes using the “relaxation sounder”, Electron DENSITY, which is capable of measuring densities in the range $0.1\text{--}100\text{ cm}^{-3}$. Thus EDEN complements MNLP which measures denser plasmas, although EDEN operates at a lower rate than MNLP. The instrument consists of a transmitter which operates in partnership with the High Frequency Receiver. In “passive mode” the transmitter is inactive and the receiver picks up natural emissions in its frequency range. Operation in active mode produces plasma resonances that are detected by the receiver, from which plasma density can be determined. Transmitter activity lasts a few seconds at a time, and is employed perhaps only once every 1 min, as it interferes with measurements from the other Fields instruments. Knowledge of the absolute electron number density is valuable for calibrating the particle instruments, cross-calibrating the magnetometer measurement (via the electron gyro-frequency), as well as for scientific studies. The method has been used in the AAR by Cluster. The transmitter frequency range will be increased for Alfvén.
- LFR** The Low Frequency Receiver provides complete information on Alfvén waves and strong double layers as well as on the wave turbulence associated with AKR and ion energisation mechanisms. The LFR digitizes 6 electric probe potentials “6xV” and 3 electric field components “3xE” from E3D as well as 3 magnetic field oscillations

from MADAM in the frequency range from DC up to 25 kHz. Using a downsampling scheme, it can provide continuous or duty cycled waveforms of these 12 quantities at various sampling rates (256 Hz, 25 kHz). It calculates their power and cross-spectra. Time resolution of the spectra can vary with mode.

4.3.8 *Electron electrostatic analyser: EESA*

The pitch angle distribution of auroral region electrons is measured at the fast rate of 40 ms, for the energy range 4 eV to 32 keV using the Electron Electro-Static Analyser instrument which consists of two sensor units, each with a top hat electrostatic analyser and an electrostatic aperture deflection system at the entrance to the top hat. The sensors must be mounted on opposite sides of the spacecraft. The field of view of the combined instrument lies in the spin plane, but can be deflected through a few 10 s of degrees as needed to ensure that it includes the magnetic field, so that continuous full pitch angle coverage is assured. There will be a total of 32 angular sectors giving pitch angle resolution of 11.25° . The geometric factor is based on the Cluster PEACE HEEA instrument, and at $1.73 \times 10^{-2} \text{ cm}^2 \cdot \text{str.eV/eV}$ is a factor 3.4 larger than for the FAST EESA (a factor 0.28 of the FAST SESA spectrograph) so that the instrument will be well optimised for auroral electron fluxes, but able to collect distributions more quickly. The time to collect a full energy-pitch angle distribution with good statistics will be 40 ms (perhaps 20 ms), i.e. at least twice as quick as FAST. In order to sweep faster the accumulation step will be 1 millisecond and there will be 40 log-spaced energy steps spaced at about $1.5 \times$ the analyser FWHM $\Delta E/E$, 16%.

4.3.9 *Ion electrostatic analyser: IESA*

The full 3D velocity distribution of ions is measured at the fast rate of 100 ms, for the energy range a few eV to 30 keV using two sensors comprising the Ion Electro-Static Analyser. The sensors must be mounted on opposite sides of the spacecraft. The technique involves a system of concentric toroidal plates with a wide effective aperture covering 2π sr solid angle coverage, that guide ions to a 2D detector plane, where arrival directions are measured with $\sim 12^\circ \times 12^\circ$ angular resolution. Energy selection is achieved using swept high voltages to provide 48 log-spaced energy channels at an energy resolution of 16%. The geometric factor of the pair of sensors is $0.1 \text{ cm}^2 \cdot \text{str.eV/eV}$, an order of magnitude larger than for the IESA on the FAST mission, allowing a time resolution of 100 ms with good counting statistics.

4.3.10 *Ion composition analyser: ICA*

The full 3D velocity distribution for several key ion species is measured at a rate of twice per spin, for the energy range a few eV to 10 keV using a single sensor Ion Composition Analyser. The instrument will distinguish

protons and oxygen ions even for weak fluxes, and will be able to resolve all major ion species (H^+ , He^+ , He^{2+} , O^+) in strong flux situations. Thus the sensor complements IESA, trading speed for simultaneous information about different ion species and finer energy resolution (10%). The instrument consists of a top hat entrance with electrostatic analyser followed by a light weight time of flight (i.e. non-magnetic) mass discrimination system which also has the advantage that the anti-coincidence system is relatively unsusceptible to false counts from penetrating radiation. The instrument is mounted on the curved face of the spacecraft, and its top hat field of view provides instantaneous $360^\circ \times 11.25^\circ$ coverage, which is swept through 4π sr during half a spacecraft spin. Typically the instrument would use 8 ms accumulation bins and a 32 step (sparse) energy sweep, collecting data from 16 anodes and 6 time-of-flight windows. The angular resolution is thus 22.5° in azimuth and 15° in polar (controlled by spin rate and energy sweep period). The geometric factor of the instrument is $8 \times 10^{-3} \text{ cm}^2 \cdot \text{sr} \cdot \text{eV/eV}$.

4.3.11 Multi-needle langmuir probes: MNLP

The electron density is measured at a rate of up to 10 kHz, over a density range of $\sim 10^2 \text{ cm}^{-3}$ to $\sim 10^6 \text{ cm}^{-3}$, (corresponding to altitudes below $\sim 3,000$ km) using a system of 3 needle probes on each of 2 booms, comprising the Multi-Needle Langmuir Probes [60]. The technique relies on the principle that probe current squared (I_e^2) plotted versus probe potential (V_p) is a straight line, of which the growth rate is proportional with the electron density squared. The quality of the electron density measurements can be judged by checking the linearity of I_e^2 versus V_p . This method is effective when the spacecraft potential is -1 to -2 V, which is expected in the relatively dense ionospheric plasma below 3,000–4,000 km altitude, but ceases to be useful in more rarefied plasma where the spacecraft potential is a few V positive (as may be confirmed using the E3D instrument). The probes are operated at a constant potential and do not generate electromagnetic noise that could affect other instruments. The probes will provide reliable data as long as they are not in the spacecraft wake. The wake extends in the direction opposite to the spacecraft velocity vector and its size varies with the local Debye length that increases with altitude (of order 1 m at altitudes between 4,000 and 5,000 km). The proposed probe mounting of probes on two booms as illustrated above is intended to ensure that at least one probe triple is always outside the wake.

4.3.12 Wide-field auroral imager: WFAI

Auroral images at UV wavelengths will be collected from the band 140–180 nm which includes the molecular N_2 Lyman-Birge-Hopfield (LBH) emissions, using the Wide Field Auroral Imager [61]. The images contain photometric information, allowing the measurement of auroral emission intensity as a function of location and time. The wide instantaneous field of view (tens of degrees) combined with the orbital motion of the platform, permits large swathes

of the auroral emission region to be observed during each spacecraft pass. The instrument sensitivity limits are between 60 Rayleigh and 20 kRayleigh. The angular resolution is ~ 15 arcminutes, hence the spatial resolution is ~ 2 km from a 500 km altitude apogee; 18 km from 4,000 km, and ~ 35 km from 8,000 km. Fields of view from each of the two planned operational orbits are illustrated in Fig. 14.

The instrument is relatively small because it uses a radially-slumped micro-channel plate optical system in conjunction with a slumped photon-counting MCP detector. The optics and detector are separated by an interference filter deposited in a CaF_2 substrate, which simultaneously selected the UV band of interest and prevents electrons reaching the detector. In particular, the filter rejects the intense Lyman- α emission at 121.6 nm, permitting auroral emission to be imaged in both the dark and sunlit ionospheres. The readout anode provides high spatial resolution at high count rates and signal processing capability within the detector. Individual photons are detected and their arrival time noted to nanosecond accuracy, easily meeting the requirement for millisecond accuracy in order to allow reconstruction of an image from a spacecraft rotating with a 6 s spin period. The instrument should be mounted with the boresight perpendicular to the rotation axis, passing through the nadir once

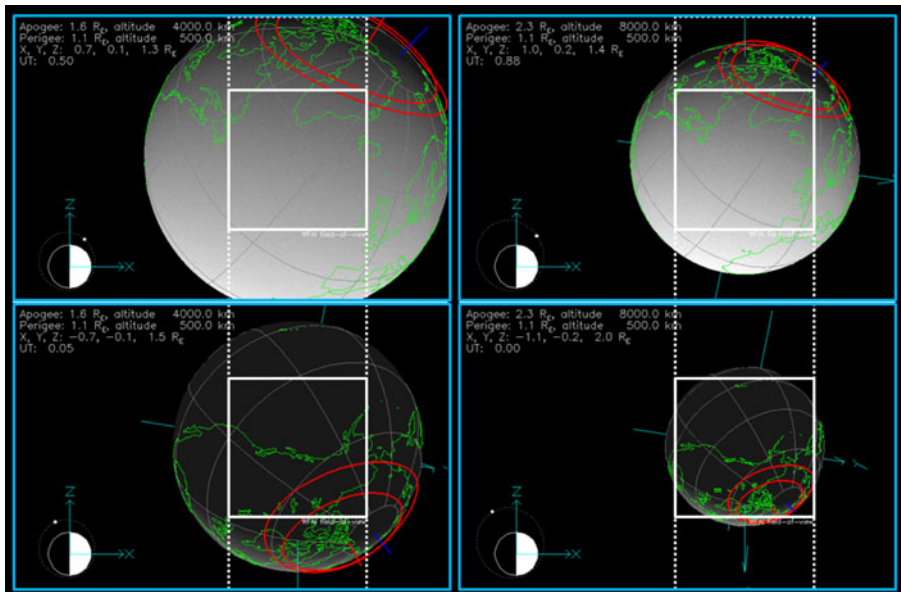


Fig. 14 Illustration of the instantaneous and swept fields of view of WFAI with the spacecraft crossing auroral magnetic field lines in the northern hemisphere, for an orbit with apogee at 60° northern latitude. The *left/right* panels show the cases of Reference Orbits 1/2, and the day/night side of the Earth is shown in the *top/bottom* row. The *solid white square* is the instantaneous field of view when pointing to the centre of the Earth. The *dotted lines* show the additional coverage due to the rotation of WFAI with the spinning spacecraft

per rotation. The spacecraft accommodation should ensure no glint affects the instrument. Spacecraft attitude knowledge accurate to a few arcmins is required, and onboard timing should be accurate to 1 millisecond resolution.

4.3.13 Data processing units

The Fields data processing unit deals with data collection and control for E3D, MAG, MADAM, HFML and CDC. It also hosts the LFR, HFR and EDEN equipment, and provides data processing, compression, and packetisation functions. The design is dual redundant. The particles data processing unit deals with data collection and control for EESA, IESA, ICA, and LMP. The system functionality includes power conversion for attached sensors, local data storage, data processing, compression, and packetisation functions. A dedicated DPU was envisaged to support the WFAI sensor. This has quite high resource requirements; a study of a significantly less resource intensive design is planned (a factor 4 lower in mass and power).

4.4 On board data handling and telemetry

Table 4 shows the proposed telemetry rate for each instrument for each of the three data collection modes; slow survey, fast survey and burst mode. A triggered 30 s HFR super high time resolution E or B waveform snapshot requiring 300 Mbit is also planned for each orbit. The total rates are comparable to those of the FAST mission, which used a similar strategy.

Table 4 Summary of payload data production rates for three rates of data collection

| Payload data rates | Slow survey kbit/s | Fast survey kbit/s | Burst kbit/s |
|-----------------------|-----------------------|-----------------------|-----------------|
| MAG | 1.54 | 1.54 | 1.54 |
| LFR DC | 3.07 | 3.07 | 3.07 |
| LFR LF | | 28.67 | 49.15 |
| LFR MF | | | 3,932.16 |
| LFR MF spectra | 4.27 | 102.40 | |
| HFR spectra | 3.20 | 6.40 | 6.40 |
| CDC | | 32.00 | 32.00 |
| EDEN | 0.20 | 0.20 | 0.20 |
| Fields/waves subtotal | 12.28 | 174.28 | 4,024.52 |
| EESA | 2.05 | 20.50 | 512.00 |
| IESA | 1.02 | 24.58 | 360.45 |
| ICA | 5.00 | 48.00 | 48.00 |
| MNLP | 0.16 | 1.60 | 16.00 |
| Particles subtotal | 8.23 | 94.68 | 936.45 |
| WFAI | 2.70 | 27.00 | 135.00 |
| Imager subtotal | 2.70 | 27.00 | 135.00 |
| TOTAL | 23.21 | 295.96 | 5,095.97 |
| FAST | 50.00 | 500.00 | 8,000.00 |

For example, using typical numbers from FAST of a 133 min period orbit and a 40 min auroral region crossing, we could consider 93 min in Slow Survey followed by the auroral region crossing of which 35 min was in Fast Survey and 5 min in Burst Mode. The accumulated data volume would be 246 Mbyte.

4.5 Requirements on the spacecraft: interfaces, pointing and alignment

The spacecraft spin axis should align with the spacecraft symmetry axis to within 0.5° to 95% confidence level (as Cluster). The spin axis should not nutate. The suggested spin period is 6 s however this parameter is flexible and should be reassessed in a detailed study phase. A shorter spin period would allow shorter intervals between imager observations of the Earth, but spin axis control becomes more difficult due to the axial E3D booms. The spin axis direction and rotation phase knowledge requirements of $\pm 0.25^\circ$ and $\pm 0.20^\circ$ are proposed based on Cluster.

The spacecraft attitude should be maintained close to the orbital plane, and to within 10° of the typical local magnetic field direction in the auroral region (magnetic latitudes 65° – 75°) in order to support auroral particle measurements. It is also important that the spacecraft attitude should be controlled when the spin plane is near the Earth-Sun line to prevent the Sun entering the line of sight of the outward facing particle and imager instruments, and to avoid the E3D probes entering shadow. The spin axis should not lie with 80° – 100° of the spacecraft-Sun vector.

No instruments require radiators or active thermal control in normal operation.

5 System requirements & key issues

The Alfvén spacecraft have identical design and construction, and identical payloads. In preparing this proposal we are guided by experience with the NASA FAST spacecraft and the ESA Cluster spacecraft. The technical implementation of the FAST mission is described in detail in several papers in Space Science Reviews, Vol 98, Nos 1–2. The FAST spacecraft operated successfully in a $350 \text{ km} \times 4,175 \text{ km}$ 83° inclination orbit, very similar to our $500 \text{ km} \times 4,000 \text{ km}$ Reference Orbit 1. Although its nominal lifetime was 1 year, its operational lifetime exceeded 10 years. Its science and payload design drivers are the same as for Alfvén, with two exceptions. Firstly, the Alfvén spacecraft will carry a wide field auroral imager. Secondly, the Alfvén spacecraft will carry sufficient fuel to alter their orbits; to vary their separation relative to one another, to modify their operational orbits and eventually to de-orbit themselves. The Cluster spacecraft flotilla have demonstrated that extensive manoeuvring, of the type we propose for Alfvén, may be done with small 10 N bipropellant thrusters. The Cluster spacecraft 400 N main engine was only used

to get from GTO to the initial operational orbit. All other manoeuvres were achieved with 10 N thrusters.

5.1 Attitude and orbit control

The preferred spacecraft attitude is with the spin axis perpendicular to the velocity vector, i.e. parallel to the orbit plane normal. Ideally the spin plane is close to the local magnetic field plane at auroral latitudes, as noted in Section 4.5. The FAST mission achieved this goal by tilting the spacecraft spin axis relative to the orbit plane normal by $\sim 3^\circ$, towards alignment with the Earth's axis, so that the magnetic field lay within $\sim 10^\circ$ of the spin plane. The arrangement is also compatible with the Alfvén auroral imager field of view requirement. All electric field boom tips should remain in sunlight. The other constraint on attitude is solar beta angle. FAST maintained this at $90^\circ \pm 30^\circ$, in order to ensure that spacecraft power and thermal constraints were respected. Depending on the design of the Alfvén spacecraft, a wider range of beta angle may be acceptable. Further study is needed to investigate how this constraint may conflict with the optimum attitude for scientific measurements, for example when the spacecraft orbit plane is perpendicular to the spacecraft-Sun line. FAST used magneto-torquers at low altitudes to achieve control of the spin axis. Attitude was sensed with a combination of a sun sensor, horizon crossing indicators and the 3 axis magnetometer.

5.2 On-board data handling and telemetry

The FAST model of data collection involved “slow survey” data collected for a large fraction of the orbit during intervals of low electron flux, “fast survey” when electron fluxes exceed a threshold, and “burst” data during short intervals when specific triggers indicating passage through regions of particular interest (and even a “high speed burst for very short intervals”). FAST used a 1 Gbit solid state recorder which is too small to contain 40 min of data collected in fast survey mode let alone burst mode, and smaller than could be downlinked in a typical contact period. Consequently the FAST team invested significant effort in onboard triggering to try to capture intervals of particular interest and managed the filling state of the recorder orbit by orbit.

Our planned telemetry levels are similar to those of FAST, and by using a similar approach we could return them in the same way (the data volume mentioned in Section 4.4 could be downlinked in a 20–30 min contact period at the maximum rate used by FAST). We propose a simpler approach, taking advantage of the larger capacity mass memory now available (8 Gbit was used on DEMETER, 32 Gbit may be realistic now) which allows us to return more complete coverage in fast survey mode with an opportunity for a fixed fraction of each auroral crossing to be collected in burst mode. In order to return the larger data volume, either a longer contact period would be used (FAST communications duration were apparently power limited, but we plan

a spacecraft with higher power) or else the following orbit would be used to complete the downlink before new science data collection occurred.

5.3 Mission operations concept (ground segment)

The mission will be operated by ESOC, with communications being handled by the ESA ground station network. The commanding and data recovery are envisaged as following the model of Cluster or Double Star, in terms of spacecraft and payload control via time tagged commands, pre-planned a few weeks ahead of execution, and regular scheduled data downlinks, ideally with onboard data storage margin to allow a second try if a downlink is interrupted or not achieved for some reason. Payload commanding will be prepared via a SOC in collaboration with PI teams. As discussed in Section 3.4 above, the precession of the line of apsides means that ground stations will be needed in both hemispheres. Figure 11 shows ground station access times determined using STK software for the two main reference orbits, using ESA ground stations at Kiruna and Perth. This confirms that the longest contact times in the $500 \times 4,000$ km orbit are of order 3,000 s (similar to FAST) and shows how ground stations in opposite hemispheres complement one another to ensure continuous availability of contact times of 2–3,000 sec (30–50 min), adequate to downlink an orbit of data with some margin. The longer period $500 \text{ km} \times 8,000 \text{ km}$ orbit offers contact times of up to 5,500 s. ESOC will collect the data from the ground stations and to make it available to PI teams via the SOC or MDC.

5.4 Estimated overall resources (mass and power)

We propose that the Alfvén spacecraft have a diameter of 2 m and a height of ~ 1 m. These dimensions are larger than FAST due to the need to accommodate fuel tanks and thrusters to facilitate orbit manoeuvres and due to the need for a larger solar panel area to support the higher planned payload average power. We also make the assumption that less highly integrated spacecraft sub-systems may be more cost-effective for an ESA mission and we seek to provide a greater degree of redundancy than was possible within the FAST design constraints. A stack consisting of a pair of 2 m diameter spacecraft, each ~ 1 m high, is consistent with the Vega launch shroud constraint.

The proposed spacecraft mass breakdown is shown in Table 5. The estimate is based on the FAST spacecraft where appropriate. Changes include (i) doubling the mass of subsystems which grow in proportion to the doubled diameter, (ii) doubling the mass of the batteries, (iii) adding 10% to other sub-systems using the recommended Design Maturity Margin principle, (iv) adding mass for fuel tanks and thrusters following the principle that their mass is 20% of the required fuel mass (as advised by Astrium engineers). In addition there is an ESA system margin of 20%.

We show in Table 5 that the planned beginning of life (BOL) solar array power is sufficient to meet the demand (including ESA system margin) after

Table 5 Summary of spacecraft subsystem mass, and of power budget. Ongoing further work shows that some of these can be reduced, for example GaAs solar array technology would allow a significant mass reduction in the solar array

| Spacecraft subsystem | Mass/kg | Spacecraft subsystem | Power/W |
|---------------------------------------|---------|-------------------------------|---------|
| Payload incl. booms | 62.28 | | |
| Mission Unique Electronics | 16.17 | <i>Power demand</i> | |
| Battery/shunt | 25.00 | Payload (all operating) | 81.11 |
| Solar array | 70.80 | Spacecraft (excl Transmitter) | 50.00 |
| ACS | 10.67 | RF system | 28.00 |
| RF system | 5.72 | <i>Subtotal</i> | 159.11 |
| Thermal system | 3.30 | ESA system margin @20% | 31.82 |
| Harness | 18.20 | TOTAL REQUIRED | 190.93 |
| Test connector panel | 0.44 | | |
| Structure | 53.00 | <i>Power supply</i> | |
| Balance weight | 10.60 | Solar array EOL | 187.2 |
| Launch adaptor | 4.00 | (ESA 20% margin on | |
| Miscellaneous | 4.40 | “BOL + 3 years”) | |
| <i>Subtotal</i> | 284.58 | Solar array EOL | 234 |
| Tanks, thrusters, pipes (20% of fuel) | 58.00 | (3 years, 10% | |
| TOTAL | 342.58 | margin = FAST actual) | |
| ESA system margin @20% | 68.52 | SOLAR ARRAY BOL REQUIRED | 260 |
| GRAND TOTAL DRY MASS | 411.10 | | |
| Fuel | 290.00 | | |
| ESA system margin @20% on fuel | 58.00 | | |
| GRAND TOTAL WET MASS | 759.10 | | |

3 years, assuming a power decline at the same rate as FAST. A slightly longer mission such as the 4 year mission we describe in Section 3 would involve a further degradation of only a few W, and does not seem an unreasonable proposition at this early stage in the mission design work. Batteries are needed to support the spacecraft during eclipses of up to 45 min duration.

5.5 Specific environmental constraints (EMC., temperature, cleanliness)

In order to minimise spacecraft disturbances to the space plasma environment and to the measurements, the spacecraft magnetic field and electric fields should be kept to a low level. Good quality “magnetic cleanliness” can be achieved by making it a design requirement on the spacecraft and payload, and by an explicit activity testing and verifying performance. Similarly, an electrostatic cleanliness programme is required. The solar array and all other spacecraft surfaces should be part of a single uniformly conducting surface in order to avoid localised areas of differential surface charging with corresponding localised electric fields. An Indium Tin Oxide coating on solar array cover glass provides the required conductivity. Other spacecraft surfaces should have a covering of conducting MLI (multi-layer insulation) that is kept electrically connected to the spacecraft structure. An electromagnetic cleanliness programme should ensure that spacecraft sub-systems do not generate

interference with measurements of high frequency electric and magnetic field disturbances due to plasma waves.

The “particles” and “imager” instruments use micro-channel plate detectors and high voltages, and require a vacuum for safe operation. During spacecraft assembly and test it is necessary to provide dry nitrogen purge for these instruments. During the initial days in orbit, time should be allowed for out-gassing before these instruments are commissioned.

Temperatures for inboard payload and spacecraft subsystems are expected to be kept within a typical range of perhaps 5° to 30°C, with a margin of order 10°C. Outboard sensors are designed for colder temperatures during normal operations and may need heaters to cope with eclipses.

5.6 Special requirements

We note that the radiation environment for this mission is relatively harsh. The Alfvén spacecraft design should take account of this. Using SPENVIS we estimate the annual dose in Reference Orbit 1 (500 km × 4,000 km, $i = 90^\circ$) as 84/48/11 krad behind the equivalent of 3/4/5 mm aluminium. The annual dose reduces to ~52/24/11 krad in Reference Orbit 2 (500 km × 8,000 km, $i = 90^\circ$) for 3/4/5 mm aluminium equivalent. For comparison, we understand that the Solar Orbiter and Bepi-Colombo mission radiation doses are ~100 krad; our 4 year mission concept dose would be similar for shielding of order 4–5 mm Aluminium. The dose behind 4 mm Aluminium is essentially the same dose tolerated by subsystems in the interior of FAST for 10 years, according to a SPENVIS analysis of the FAST orbit. The longevity of the FAST spacecraft demonstrates the success of the FAST design approach which could serve as a model for Alfvén.

6 Technology development, programmatic and cost

6.1 Technology development requirements

No major spacecraft design challenges are foreseen, as all relevant technologies have already been demonstrated by mission such as FAST, THEMIS, Cluster and the soon-to-be launched MMS. Similarly, payload technology development requirements are rather minor. All the payload will be at TRL5 by 2012 and all apart from IESA and WFAI have extensive flight heritage.

6.2 Overall mission cost analysis

Although detailed mission cost estimates are difficult, especially at such a preliminary stage, we note that following ESA’s guidelines for an initial estimate, our mission concept cost falls well inside the ESA M3 mission cost cap.

6.3 Mission schedule drivers, risks and alternate strategies

There are no mission design related schedule drivers. The launch date is relatively flexible and not tied to narrow launch windows as might be the case for example for a typical planetary mission. Due to the low technical risk associated with the payload and the spacecraft designs, the mission could be carried out on the timescale envisaged for the ESA M3 mission, leading to a launch as early as late 2020.

7 Communication and outreach

The aurora borealis or “northern lights” have captivated onlookers since the earliest humans arrived in the polar regions. Cultures around the arctic circle have developed a range of myths and folklore in order to explain the appearance of these ghostly lights in the night sky and this keen interest in one of nature’s most spectacular natural phenomenon continues to the present day. The aurora regularly appears in popular culture through film, television and literature while an entire industry has developed to enable tourists to view the northern lights first-hand from cruise liners, pleasure flights and arctic holidays.

8 Conclusions

The Alfvén mission concept is designed to make a major step forward in understanding the plasma physics processes that ultimately generate the beautiful ever-changing aurora. These processes are not well understood and their study will produce insights with applicability across a wide range of astrophysical phenomena. A multi-spacecraft mission with sufficiently fast fields and particles instrumentation is essential to meet this goal.

The strong scientific return outlined in this paper can be achieved using a two spacecraft mission which could be implemented quickly, costs significantly less than the ESA Medium Class mission cost cap, does not rely on international partnerships and which does not involve technological risks that might later drive up costs or introduce programme delays.

In closing, we note that a three spacecraft mission, likely also affordable within the ESA M3 cost cap, was also studied but is not reported here. The concept offers greater insurance against the risk of instrument or spacecraft problems, and improved science return in some areas.

Acknowledgements Special thanks are due to the CNES/PASO team and EADS Astrium UK for their contributions. We thank Viktor Doychinov for his (post-proposal) UCL Masters degree project work which made a detailed study of some Alfvén spacecraft sub-systems and confirmed the communications concept. All participants gratefully acknowledge the various funding bodies which supported their work.

References

1. Chaston, C.C., et al.: How important are dispersive Alfvén waves for auroral particle acceleration? *Geophys. Res. Lett.* **34** (2007). doi:[10.1029/2006GL029144](https://doi.org/10.1029/2006GL029144)
2. Dombeck, J.C., et al.: Alfvén waves and Poynting flux observed simultaneously by Polar and FAST in the plasma sheet boundary layer. *J. Geophys. Res.* **110** (2005). doi:[10.1029/2005JA011269](https://doi.org/10.1029/2005JA011269)
3. Chaston, C.C., et al.: FAST observations of inertial Alfvén waves in the dayside aurora. *Geophys. Res. Lett.* **26**, 647–650 (1999)
4. Watt, C.E.J., Rankin, R.: Electron trapping in shear Alfvén waves that power the Aurora. *Phys. Rev. Lett.* **102**, 045002 (2009)
5. Chaston, C.C., et al.: Width and brightness of auroral arcs driven by inertial Alfvén waves. *J. Geophys. Res.* **108** (2003). doi:[10.1029/2001JA007537](https://doi.org/10.1029/2001JA007537)
6. Stasiewicz, K., et al.: Identification of widespread turbulence of dispersive Alfvén waves. *Geophys. Res. Lett.* **27**, 173–176 (2000)
7. Haerendel, G., Cosmic linear accelerators. In: Proc. of the International School and Workshop on Plasma Astrophysics, pp. 37–44. ESA SP-285, ESA, Noordwijk (1989)
8. Génot, V., et al.: A study of the propagation of Alfvén waves in the auroral density cavities. *J. Geophys. Res.* **104**, 22649–22656 (1999)
9. Génot, V., et al.: Alfvén wave interaction with inhomogeneous plasmas: acceleration and energy cascade towards small-scales. *Ann. Geophys.* **22**, 2081–2096 (2004)
10. Chaston, C.C., et al.: Ionospheric erosion by Alfvén waves. *J. Geophys. Res.* **111** (2006). doi:[10.1029/2005JA011367](https://doi.org/10.1029/2005JA011367)
11. Akasofu, S.: The development of the auroral substorm. *Planet. Space Sci.* **12**, 273–282 (1964)
12. Lui, A.T.Y.: A synthesis of magnetospheric substorm models. *J. Geophys. Res.* **96**, 1849–1856 (1991)
13. Mende, S., et al.: FAST and IMAGE-FUV observations of a substorm onset. *J. Geophys. Res.* **108** (2003). doi:[10.1029/2002JA009787](https://doi.org/10.1029/2002JA009787)
14. Newell, P.: Substorm cycle dependence of various types of aurora. *J. Geophys. Res.* **115** (2010). doi:[10.1029/2010JA015331](https://doi.org/10.1029/2010JA015331)
15. Rae, I.J., et al.: Optical characterization of the growth and spatial structure of a substorm onset arc. *J. Geophys. Res.* **115** (2010). doi:[10.1029/2010JA015376](https://doi.org/10.1029/2010JA015376)
16. Rae, I.J., et al.: Timing and localization of ionospheric signatures associated with substorm expansion phase onset. *J. Geophys. Res.* **114** (2009). doi:[10.1029/2008JA013559](https://doi.org/10.1029/2008JA013559)
17. Morioka, A., et al.: Vertical evolution of the auroral acceleration at substorm onset. *Ann. Geophys.* **27**, 525–535 (2009)
18. Newman, D., et al.: Dynamics and instability of electron phase-space tubes. *Phys. Rev. Lett.* **86**, 1239–1242 (2001)
19. Goldman, M., et al.: Phase-space holes due to electron and ion beams accelerated by a current-driven potential ramp. *Nonlinear Process. Geophys.* **10**, 37–44 (2003)
20. Chiu, Y.T., Schultz, M.: Self-consistent particle and parallel electrostatic field distributions in magnetospheric-ionospheric auroral region. *J. Geophys. Res.* **83**, 629–642 (1978)
21. Ergun, R.E., et al.: Parallel electric fields in the upward current region of the aurora. *Phys. Plasmas* **9**, 3695–3704 (2002)
22. Knight, S.: Parallel electric fields. *Planet. Space Sci.* **21**, 741–750 (1973)
23. McFadden, J., et al.: FAST observations of ion solitary waves. *J. Geophys. Res.* **108** (2003). doi:[10.1029/2002JA009485](https://doi.org/10.1029/2002JA009485)
24. Muschietti, L., Roth, I.: Ion two-stream instabilities in the auroral acceleration zone. *J. Geophys. Res.* **113** (2008). doi:[10.1029/2007JA013005](https://doi.org/10.1029/2007JA013005)
25. Muschietti, L., et al.: Phase-space electron holes along magnetic field lines. *Geophys. Res. Lett.* **26**, 1093–1096 (1999)
26. Berthomier, M., et al.: Stability of three-dimensional electron holes. *Phys. Plasmas* **15** (2008). doi:[10.1063/1.3013452](https://doi.org/10.1063/1.3013452)
27. Ergun, R.E., et al.: Electron phase-space holes and the VLF saucer source region. *Geophys. Res. Lett.* **28**, 3805–3808 (2001)
28. Ergun, R.E., et al.: FAST satellite wave observations in the AKR source region. *Geophys. Res. Lett.* **25**, 2061–2064 (1998)

29. Wu, C.S., Lee, L.C.: Theory of the terrestrial kilometric radiation. *Astrophys. J.* **230**, 621–626 (1979)
30. Louarn, P., et al.: Trapped electrons as the free energy source for auroral kilometric radiation. *J. Geophys. Res.* **95**, 5983–5993 (1990)
31. Ergun, R.E., et al.: Electron cyclotron maser driven by charged particle acceleration from magnetic-field aligned electric fields. *Astrophys. J.* **538**, 456–474 (2000)
32. Panchenko, M., et al.: Estimation of linear wave polarization of the auroral kilometric radiation. *Radio Sci.* **43**, RS1006 (2008)
33. Louarn, P., Le Quéau, D.: Generation of the auroral kilometric radiation in plasma cavities. *Planet. Space Sci.* **44**, 199–224 (1996)
34. Pottelle, R., et al.: Auroral plasma turbulence and the cause of AKR fine structure. *J. Geophys. Res.* **106**, 8465–8476 (2001)
35. Mutel, R.L., et al.: Striated auroral kilometric radiation emission: a remote tracer of ion solitary structures. *J. Geophys. Res.* **111**, A10203 (2006)
36. Pottelle, R., et al.: Electrostatic shock properties inferred from AKR fine structure. *Nonlinear Process. Geophys.* **10**, 87–92 (2003)
37. Hess, S., et al.: Jovian S-burst generation by Alfvén waves. *J. Geophys. Res.* **112**, A11212 (2007)
38. Su, Y., et al.: Short-burst auroral radiations in Alfvénic acceleration regions: FAST observations. *J. Geophys. Res.* **113**, A08214 (2008)
39. Zarka, P.: Radio and plasma waves at the outer planets. *Adv. Space Res.* **33**, 2045–2060 (2004)
40. Lamy, L., et al.: Properties of Saturn kilometric radiation measured within its source region. *Geophys. Res. Lett.* **37**, L12104 (2010)
41. Jackman, C.M., Lamy, L., Freeman, M.P., Zarka, P., Cecconi, B., Kurth, W.S., Cowley, S.W.H., Dougherty, M.K.: On the character and distribution of lower-frequency radio emissions at Saturn and their relationship to substorm-like events. *J. Geophys. Res.* **114**, A08211 (2009). doi:[10.1029/2008JA013997](https://doi.org/10.1029/2008JA013997)
42. Treumann, R.A.: The electron cyclotron maser for astrophysical applications. *Astron. Astrophys. Rev.* **13**, 229–315 (2006)
43. Zarka, P.: Plasma interactions of exoplanets with their parent star and associated radio emissions. *Planet. Space Sci.* **55**, 598–617 (2007)
44. Magnetospheric plasma sources and losses, chapter 2. In: Hultqvist, B., Oieroset, M., Paschmann, G., Treumann, R. (eds.) *ISSI Space Sciences Series*, vol 6. Kluwer Academic Publishers (1999)
45. Kistler, L., et al.: Cusp as a source for oxygen in the plasma sheet during geomagnetic storms. *J. Geophys. Res.* **115** (2010). doi:[10.1029/2009JA014838](https://doi.org/10.1029/2009JA014838)
46. Moen, J., et al.: On the relationship between ion upflow events and cusp auroral transients. *Geophys. Res. Lett.* **31** (2004). doi:[10.1029/2004GL020129](https://doi.org/10.1029/2004GL020129)
47. Barabash, S., et al.: Martian atmospheric erosion rates. *Science* **315**, 501–503 (2007)
48. Nilsson, H., et al.: The ionospheric signature of the cusp as seen by incoherent scatter radar. *J. Geophys. Res.* **101**, 10947–10963 (1996)
49. Strangeway, R.J., et al.: Factors controlling ionospheric outflows as observed at intermediate altitudes. *J. Geophys. Res.* **110** (2005). doi:[10.1029/2004JA010829](https://doi.org/10.1029/2004JA010829)
50. André, M., et al.: Ion energization mechanisms at 1700 km in the auroral region. *J. Geophys. Res.* **103**, 4199–4122 (1998)
51. Chaston, C.C., et al.: Auroral ion acceleration in dispersive Alfvén waves. *J. Geophys. Res.* **109** (2004). doi:[10.1029/2003JA010053](https://doi.org/10.1029/2003JA010053)
52. Cattell, C., et al.: The association of electrostatic ion cyclotron waves, ion and electron beams and field-aligned currents: FAST observations of an auroral zone crossing near midnight. *Geophys. Res. Lett.* **25**, 2053–2056 (1998)
53. Vago, J.L., et al.: Transverse ion acceleration by localized lower hybrid waves in the topside ionosphere. *J. Geophys. Res.* **97**, 16935–16957 (1992)
54. Nilsson, H., et al.: An assessment of the role of the centrifugal acceleration mechanism in high altitude polar cap oxygen ion outflow. *Ann. Geophys.* **26**, 145–157 (2008)
55. Newell, P., Lyons, K., Meng, C.: A large survey of electron acceleration events. *J. Geophys. Res.* **101**, 2599 (1996)
56. Paschmann, G., Haaland, S., Treumann, R. (eds.): *Auroral Plasma Physics*, Chapter 5. *ISSI Space Science Series Vol 15*. Kluwer Academic Publishers (2003)

57. Sandahl, I. (ed.): In *The Light of the Aurora, Optical Research in Northernmost Europe*. TemaNord 2009:557, Nordic Council of Ministers, Copenhagen (2009)
58. Cavoit, C.: Closed loop applied to magnetic measurements in the range of 0.1–50 MHz. *Rev. Sci. Instrum.* **77**, 064703 (2006). doi:[10.1063/1.2214693](https://doi.org/10.1063/1.2214693)
59. Krasnoselskikh, V.V., Natanzon, A.M., Reznikov, A.E., Schyokotov, A.Y., Klimov, S.I., Kruglyi, A.E., Woolliscroft, L.J.C.: Current measurements in space plasmas and the problem of separating between spatial and temporal variations in the field of a plane electromagnetic wave. *Adv. Space Res.* **11**(9), 37–40 (1991)
60. Bekkeng, T.A., Jacobsen, K.S., Bekkeng, J.K., Pedersen, A., Lindem, T., Lebreton, J.-P., Moen, J.I.: Design of a novel multi-needle Langmuir probe system. *Meas. Sci. Technol.* **21**, 085903 (2010). doi:[10.1088/0957-0233/21/8/085903](https://doi.org/10.1088/0957-0233/21/8/085903)
61. Bannister, N.P., Bunce, E.J., Cowley, S.W.H., Fairbend, R., Fraser, G.W., Hamilton, F.J., Lapington, J.S., Lees, J.E., Lester, M., Milan, S.E., Pearson, J.F., Price, G.J., Willingale, R.: A Wide Field Auroral Imager (WFAI) for low earth orbit missions. *Ann. Geophys.* **25**, 519 (2007)